Structural basis of resistance to lincosamide, streptogramin A, and pleuromutilin antibiotics by ABCF ATPases in Gram-positive pathogens

Caillan Crowe-McAuliffe[1,#], Victoriia Murina[2,3,#], Kathryn Jane Turnbull[2,3], Marje Kasari[4] Merianne Mohamad[5], Christine Polte[1], Hiraku Takada[2,3], Karolis Vaitkevicius[2,3], Jörgen Johansson[2,3], Zoya Ignatova[1], Gemma C. Atkinson[2], Alex J. O'Neill[5], Vasili Hauryliuk[2,3,4*], Daniel N. Wilson[1*]

[1] Institute for Biochemistry and Molecular Biology, University of Hamburg, Martin-Luther-King-Platz 6, 20146 Hamburg, Germany.

[2] Department of Molecular Biology, Umeå University, 90187 Umeå, Sweden.

[3] Laboratory for Molecular Infection Medicine Sweden (MIMS), Umeå University, 90187 Umeå, Sweden.

[4] University of Tartu, Institute of Technology, 50411 Tartu, Estonia.

[5] Astbury Centre for Structural Molecular Biology, School of Molecular & Cellular Biology, Faculty of Biological Sciences, University of Leeds, Leeds LS2 9JT, UK.

[#] These authors contributed equally.

*Correspondence to: Daniel.Wilson@chemie.uni-hamburg.de, vasili.hauryliuk@umu.se.

Abstract

Target protection proteins bind to antibiotic targets and confer resistance to the host organism. One class of such proteins, termed antibiotic resistance (ARE) ATP binding cassette (ABC) proteins of the F-subtype (ARE ABCFs), are widely distributed throughout Gram-positive bacteria and bind the ribosome to alleviate translational inhibition by antibiotics that target the large ribosomal subunit. Using single-particle cryo-EM, we have solved the structure of ARE ABCF–ribosome complexes from three Gram-positive pathogens: *Enterococcus faecalis* LsaA, *Staphylococcus haemolyticus* $VgaA_{LC}$ and *Listeria monocytogenes* VgaL. Supported by extensive mutagenesis analysis, these structures enable a comparative approach to understanding how these proteins mediate antibiotic resistance on the ribosome. We present evidence of mechanistically diverse allosteric relays converging on a few peptidyltransferase center (PTC) nucleotides, and propose a general model of antibiotic resistance mediated by these ARE ABCFs.

Introduction

The bacterial ribosome is a major antibiotic target (Wilson, 2014). Despite the large size of the ribosome, and the chemical diversity of ribosome-targeting small compounds, only a few sites on the ribosome are known to be bound by clinically-used antibiotics. On the 50S large ribosomal subunit, two of the major antibiotic binding sites are the peptidyltransferase center (PTC) and the nascent peptide exit tunnel. The PTC is targeted by pleuromutilin, streptogramin A, and lincosamide (PS_AL) antibiotics, as well as phenicols and oxazolidinones (Dunkle *et al*, 2010; Matzov *et al*, 2017; Schlünzen *et al*, 2004; Tu *et al*, 2005; Wilson *et al*, 2008). Representatives of macrolide and streptogramin B classes bind at adjacent sites at the beginning of the nascent peptide exit tunnel (Dunkle *et al.*, 2010; Tu *et al.*, 2005).

Many mechanisms have evolved to overcome growth inhibition by such antibiotics in bacteria, among them target protection mediated by a subset of ABC family of proteins (Wilson *et al*, 2020). ATP-binding cassette (ABC) ATPases are a ubiquitous superfamily of proteins found in all domains of life, best-known as components of membrane transporters (Krishnan *et al*, 2020; Rees *et al*, 2009). A typical ABC transporter contains two nucleotide-binding domains (NBDs), each of which contribute one of two faces to an ATP-binding pocket, as well as transmembrane domains (Thomas & Tampé, 2020). Some sub-groups of ABC proteins, however, lack membrane-spanning regions and have alternative cytoplasmic functions, such as being involved in translation (Davidson *et al*, 2008; Fostier *et al*, 2020; Gerovac & Tampé, 2019). For example, in eukaryotes Rli1/ABCE1 is a ribosome splitting factor involved in recycling after translation termination, and the fungal eEF3 proteins bind the ribosome to facilitate late steps of translocation and E-site tRNA release (Andersen *et al*, 2006; Ranjan *et al*, 2020). The F-type subfamily of ABC proteins, which are present in bacteria and eukaryotes, contain at least two NBDs separated by an α-helical interdomain linker and notably lack transmembrane regions (Murina *et al*, 2019; Ousalem *et al*, 2019).

One group of bacterial ABCFs, which are termed antibiotic resistance (ARE) ABCFs (Dorrian & Kerr, 2009), confer resistance to antibiotics that bind to the 50S subunit of the bacterial ribosome (Ero *et al*, 2019; Ousalem *et al.*, 2019; Sharkey & O'Neill, 2018; Wilson *et al.*, 2020). Characterized ARE ABCFs are found predominantly in Gram-positive bacteria, including human and animal pathogens, typically have a restricted host specificity, and can be further divided into eight subfamilies (Allignet *et al*, 1992; Murina *et al.*, 2019; Wilson *et al.*, 2020). Although initially thought to act as part of efflux systems (Ross *et al*, 1990; Ross *et al*, 1989), these proteins were subsequently shown instead to bind the ribosome, oppose antibiotic binding, and to reverse antibiotic-mediated translation inhibition of translation *in vitro* (Sharkey *et al*, 2016).

Phylogenetic analyses indicate that ARE ABCFs may have arisen multiple times through convergent evolution, and that antibiotic specificity can be divergent within a related subgroup (Murina *et al.*, 2019). Classified by the spectrum of conferred antibiotic resistance, ARE ABCFs can be categorized into three groups (Murina *et al.*, 2019; Sharkey & O'Neill, 2018):

1. A highly polyphyletic group of ARE ABCFs that confer resistance to the PTC-binding PS_AL antibiotics (ARE1, ARE2, ARE3, ARE5 and ARE6 subfamilies). The most well-studied representatives are VmlR, VgaA, SalA, LmrC and LsaA (Allignet *et al.*, 1992; Hot *et al*, 2014; Koberska *et al*, 2020; Ohki *et al*, 2005; Singh *et al*, 2002). Additionally, a lincomycin-resistance ABCF that belongs to this group, termed Lmo0919, has been reported in *Listeria monocytogenes* (Chesneau *et al*, 2005; Dar *et al*, 2016; Duval *et al*, 2018).
2. ARE ABCFs that confer resistance to antibiotics that bind within the nascent peptide exit channel (a subset of the ARE1 subfamily, and ARE4). The most well-studied representatives are Macrolide and streptogramin B resistance (Msr) proteins (Reynolds & Cove, 2005; Ross *et al.*, 1990; Su *et al*, 2018).
3. Poorly experimentally characterized ARE ABCF belonging to subfamilies ARE7 (such as OptrA) and ARE8 (PoxtA). These resistance factors confer resistance to phenicols and oxazolidinones that bind in the PTC overlapping with the PS_AL binding site (Antonelli *et al*, 2018; Wang *et al*, 2015; Wilson *et al.*, 2020) and are spreading rapidly throughout bacteria in humans and livestock by horizontal gene transfer (Freitas *et al*, 2017; Iimura *et al*, 2020; Sadowy, 2018; Zhang *et al*, 2020).

Additionally, several largely unexplored groups of predicted novel ARE ABCFs are found in high-GC Gram-positive bacteria associated with antibiotic production (Murina *et al.*, 2019).

So far, two structures of ARE ABCFs bound to the 70S ribosome have been determined (Crowe-McAuliffe *et al*, 2018; Ero *et al.*, 2019; Su *et al.*, 2018). In each instance, the ARE ABCF interdomain linker extended from the E-site-bound NBDs into the relevant antibiotic-binding site in the ribosome, distorting the P-site tRNA into an unusual state in the process. The tip of the interdomain linker—termed the antibiotic resistance determinant (ARD)—is not well conserved among (or sometimes even within) subfamilies, and mutations in this region can abolish activity as well as change antibiotic specificity. Mutagenesis indicates that both steric overlap between the ARD and the antibiotic, as well as allosteric reconfiguration of the rRNA and the antibiotic-binding site, may contribute to antibiotic resistance (Crowe-McAuliffe *et al.*, 2018; Ero *et al.*, 2019; Lenart *et al*, 2015; Su *et al.*, 2018). Non-ARE ribosome-associated ABCFs that do not confer resistance to antibiotics—such as EttA—tend to have

relatively short interdomain linkers that contact and stabilize the P-site tRNA (Chen *et al*, 2014). ARE ABCFs that confer resistance to PS_AL antibiotics (such as VmlR) have extensions in the interdomain linker that allow them to reach into the antibiotic-binding site in the PTC (Chen *et al.*, 2014; Crowe-McAuliffe *et al.*, 2018; Lenart *et al.*, 2015). The longest interdomain linkers belong to ARE ABCFs that confer resistance to macrolides and streptogramin Bs (e.g. MsrE), and such linkers can extend past the PTC into the nascent peptide exit tunnel (Su *et al.*, 2018). The length of the bacterial ABCF ARD generally correlates with the spectrum of conferred antibiotic resistance. Notable exceptions to this pattern are OptrA and PoxtA ARE ABCF which have short interdomain linkers, yet still confer resistance to some PTC-binding antibiotics (Antonelli *et al.*, 2018; Wang *et al.*, 2015), while typically PTC-protecting ARE ABCFs such as VmlR, LsaA and VgaA, typically have comparatively long interdomain linkers (Lenart *et al.*, 2015; Singh *et al*, 2001).

The available ARE ABCF-ribosome structures were generated by *in vitro* reconstitution. *Pseudomonas aeruginosa* MsrE, which confers resistance to tunnel-binding macrolides and streptogramin Bs (that inhibit translation elongation) was analyzed bound to a heterologous *Thermus thermophilus* initiation complex (Su *et al.*, 2018). *Bacillus subtilis* VmlR, which confers resistance to PS_AL antibiotics that bind in the PTC (which stall translation at initiation) was analyzed in complex with an *B. subtilis* 70S ribosome arrested during elongation by the presence of a macrolide antibiotic (Crowe-McAuliffe *et al.*, 2018; Dornhelm & Högenauer, 1978; Meydan *et al*, 2019; Ohki *et al.*, 2005; Orelle *et al*, 2013). Structures of native physiological complexes (such as those generated using pull-down approaches from the native host) are currently lacking.

Here we have thoroughly characterized the antibiotic resistance specificity and determined the structure of three native ARE ABCF-70S ribosome complexes using affinity chromatography and cryo-electron microscopy (cryo-EM). We selected ARE ABCFs that confer resistance to PS_AL antibiotics in clinically-relevant Gram-positive pathogens: ARE3 representative *Enterococcus faecalis* LsaA (Singh *et al.*, 2002), and ARE1 representatives *Listeria monocytogenes* Lmo0919 (Chesneau *et al.*, 2005; Dar *et al.*, 2016; Duval *et al.*, 2018)—which we have termed VgaL—as well as the well-characterized $VgaA_{LC}$ protein, initially isolated from *Staphylococcus haemolyticus* (Allignet *et al.*, 1992; Chesneau *et al.*, 2005; Jacquet *et al*, 2008; Lenart *et al.*, 2015; Novotna & Janata, 2006). *Staphylococcus* and *Enterococcus* are commensal organisms that are prevalent in diverse healthcare-associated infections, and antibiotic resistance is spreading through these species (Magill *et al*, 2014; Mamtora *et al*, 2019; Mendes *et al*, 2019; Pfaller *et al*, 2019). *L. monocytogenes* is a foodborne pathogen that poses particular risk to pregnant women and immunocompromised patients (Camargo *et al*, 2016). Our structures, supported by extensive mutagenesis

143 experiments, provide much needed insight into the mechanism by which these distinct ARE
144 ABCFs displace antibiotics from their binding site on the ribosome to confer antibiotic
145 resistance.

Results

Cryo-EM structures of native ARE ABCF-70S complexes

To obtain native ARE ABCF-70S complexes, we expressed C-terminally $FLAG_3$-tagged ATPase-deficient EQ_2 variants of *E. faecalis* LsaA, *S. aureus* $VgaA_{LC}$, and *L. monocytogenes* VgaL in their corresponding native host bacterial species. The $FLAG_3$ tag was used for affinity purification of each protein locked on the ribosomal target. The ARE ABCFs co-migrated with the 70S fraction through sucrose gradients—with the complex further stabilized in the presence of ATP in the case of LsaA and $VgaA_{LC}$—and co-eluted with ribosomal proteins after affinity purification (Figures S1–3).

The resulting native complexes were characterized by single-particle cryo-EM (see Methods), yielding ARE–70S complexes with average resolutions of 2.9 Å for *E. faecalis* LsaA, 3.1 Å for *S. aureus* $VgaA_{LC}$, and 2.9 Å for *L. monocytogenes* VgaL (Figure 1A-C, Table S4, Figures S4–S6). In each instance, the globular nucleotide-binding domains (NBDs) of the ARE ABCF bound in the E-site, and the α-helical interdomain linker extended towards the peptidyl-transferase center (PTC, Figure 1A–C). Additionally, a distorted tRNA occupied the P-site (Figure 1A–C), similarly to what was observed previously for *P. aeruginosa* MsrE and *B. subtilis* VmlR (Crowe-McAuliffe *et al.*, 2018; Su *et al.*, 2018). For the LsaA and VgaL samples, occupancy of the factor on the ribosome was high, with >95% or ~70% of picked ribosomal particles containing LsaA or VgaL, respectively (Figures S4 and S6). By contrast, $VgaA_{LC}$ had lower occupancy (~60%), implying that the factor dissociated after purification and/or during grid preparation (Figure S5). *In silico* 3D classification revealed that the major class not containing $VgaA_{LC}$ in the dataset was a 70S ribosome with P-tRNA, which could also be refined to an average resolution of 3.1 Å (Figure S5). Generally, the 50S ribosomal subunit and ARE ABCF interdomain linkers were well-resolved (Figures 1D–F and S4–S6). While ARE ABCF NBDs, occupying the E site, had a lower resolution—especially in the regions that contact the ribosomal L1 stalk and the 30S subunit—the density was nonetheless sufficient to dock and adjust homology models in each instance (Figures 1D–F and S4–S6). Densities corresponding to the 30S subunits were less clear, indicating flexibility in this region, but nonetheless sufficient to build near-complete models of each ribosome. Density corresponding to ATP and a coordinated magnesium ion was observed in both nucleotide-binding sites for each ARE ABCF (Figure 1D–F and S7). Density for the ATP bound in the peripheral nucleotide-binding site was relatively poor, with little density corresponding to the nucleobase moiety, consistent with the relaxed nucleotide specificity of these proteins (Figure S7) (Murina *et al*, 2018).

By comparison to structures of other ABC proteins, the NBDs adopted a closed conformation bound tightly to each nucleotide (Figure S8). In each ARE ABCF–70S map, the acceptor stem of the P-site tRNA was distorted, as observed previously for MsrE and VmlR (Crowe-McAuliffe *et al.*, 2018; Su *et al.*, 2018). The CCA 3′ end was particularly disordered, precluding any additional density corresponding to an amino acid or nascent chain from being visualized (Figures 1A-C and S4–S6). To our knowledge, this is the first model of the ribosome from the Gram-positive pathogen *L. monocytogenes* that have been described. Additionally, we have used our high-resolution map to create an updated model of the *S. aureus* ribosome (Khusainov *et al*, 2016). Our models of the *E. faecalis* and *S. aureus* ribosomes are generally in agreement with those recently described (Golubev *et al*, 2020; Murphy *et al*, 2020).

LsaA, Vga_{LC} and VgaL bind to translation initiation states

In each cryo-EM map, the P-site tRNA body was sufficiently well-resolved so as to unambiguously assign the density to initiator $tRNA^{fMet}$, on the basis of (i) general fit between sequence and density, (ii) the well-resolved codon-anticodon interaction, and (iii) a characteristic stretch of G:C base pairs found in the anticodon stem loop of $tRNA^{fMet}$ (Figure 2A–C). Additionally, in the small subunit mRNA exit tunnel, density corresponding to a putative Shine-Dalgarno–anti-Shine-Dalgarno helix was observed, consistent with the ARE ABCF binding to an initiation complex containing $tRNA^{fMet}$ (Figure 2D). LsaA–*E. faecalis* 70S samples were further analyzed with a custom tRNA microarray, which confirmed $tRNA^{fMet}$ was the dominant species found in the sample (Figure 2E). Collectively, these observations indicate that in our structures the majority of the ARE ABCFs are bound to 70S translation initiation complexes.

Further examination of the LsaA–70S volume revealed weak density in the ribosomal A site (Figure S4F), suggesting that some complexes had entered into the first elongation cycle. This was unexpected, as the distorted P-site tRNA is predicted to overlap with an accommodated A-site tRNA, although as noted would be compatible with a pre-accommodated A/T-tRNA (Crowe-McAuliffe *et al.*, 2018). A mask around the A site was used for partial signal subtraction, and focused 3D classification was used to further sub-sort the LsaA–70S volume. One class, containing approximately one third of the particles, was shown to indeed contain a tRNA in the A site (Figures S4, S9A). This tRNA was poorly resolved, suggesting flexibility, and was slightly rotated compared to a canonical, fully accommodated A-site tRNA, and, as for the P-site tRNA, the acceptor stem was significantly disordered and displaced (Figure S9B,C). This state likely reflects an incomplete or late-intermediate

accommodation event, as observed previously when translation is inhibited by PTC binding antibiotics hygromycin A or A201A, both of which were shown to sterically exclude the acceptor stem of a canonical A-site tRNA (Polikanov *et al*, 2015). A very weak density corresponding to an A-site tRNA was also observed in $VgaA_{LC}$ and VgaL volumes, but sub-classification was unsuccessful for these datasets.

$VgaA_{LC}$ and VgaL, both of which belong to the ARE1 subfamily—although not LsaA, which belongs to the ARE3 subfamily—contain a short C-terminal extension predicted to form two α-helices (Crowe-McAuliffe *et al.*, 2018; Murina *et al.*, 2019). Although not conserved among all AREs, deletion of the CTE abolished antibiotic resistance in VmlR and reduces antibiotic resistance in VgaA, implying that this extension is necessary for function in some ARE ABCFs (Crowe-McAuliffe *et al.*, 2018; Jacquet *et al.*, 2008). Density for this region, which emanates from NBD2 and was located between ribosomal proteins uS7 and uS11, was present in the $VgaA_{LC}$–70S and VgaL–70S maps and was essentially consistent with the position of the VmlR C-terminal extension, although was not sufficiently resolved to create a model for this region. Although bound close to the mRNA exit channel, the CTEs of $VgaA_{LC}$ and VgaL did not contact the Shine-Dalgarno–anti-Sine-Dalgarno helix of the initiation complexes, indicating they are not critical for substrate recognition in these ARE ABCFs (Figure S10).

The location and conformation of short and long ARDs on the ribosome

The ARD loop, positioned between the two long α-helices that link the NBDs, is a critical determinant of antibiotic resistance (Crowe-McAuliffe *et al.*, 2018; Lenart *et al.*, 2015; Murina *et al.*, 2018; Sharkey *et al.*, 2016; Su *et al.*, 2018). Despite sharing a similar antibiotic specificity profile, the ARDs of LsaA, $VgaA_{LC}$, VgaL, and VmlR are divergent in both amino acid composition and length, which is consistent with the polyphyletic nature of this group but precludes confident sequence alignment of this region (Figure 3A). Despite such sequence divergence, the position of the ARDs on the ribosome is broadly similar in each instance (Figure 3B–G). By comparison to tiamulin, which overlaps with the aminoacyl moieties of A- and P-tRNAs in the PTC, VmlR, LsaA, $VgaA_{LC}$, and VgaL are all positioned similarly on the ribosome, with the ARD backbone adjacent to the antibiotic binding site (Figure 3B–F) (Polikanov *et al.*, 2015; Schlünzen *et al.*, 2004). Compared to VmlR, the additional residues in the ARDs of LsaA, $VgaA_{LC}$, and VgaL extend away from the antibiotic binding site, towards the CCA 3′ end of the distorted P-tRNA (Figure 3C–F). By contrast, MsrE, which confers resistance to tunnel-binding antibiotics deeper in the ribosome, has a longer ARD that extends both past the PTC to approach the macrolide/streptogramin A binding site, as well as towards the distorted P-tRNA (Figure 3A, G) (Dunkle *et al.*, 2010; Su *et al.*, 2018). Thus,

the length of the ARD does not necessarily provide insights into the extent to which the ARD will extend into the ribosomal tunnel and thus one cannot easily predict whether long ARDs will confer resistance to macrolide antibiotics.

Position of the ARDs with respect to PS_AL antibiotic binding site

We next made a careful comparison of the LsaA, $VgaA_{LC}$, and VgaL ARDs with the binding sites of relevant antibiotics within the PTC (Figure 4A, B) (Dunkle *et al.*, 2010; Matzov *et al.*, 2017; Schlünzen *et al.*, 2004; Tu *et al.*, 2005). For LsaA, the side chain of Phe257 overlapped with the binding sites of tiamulin, virginiamycin M, and lincomycin, but was not close to erythromycin (Figure 4A–C), consistent with the spectrum of antibiotic resistance conferred by this protein (Table S1). In the $VgaA_{LC}$ ARD, Val219 was situated close to tiamulin and virginiamycin M, and had a modest predicted overlap with lincomycin (Figure 4D). Notably, in the closely related variant VgaA, which has a similar specificity with modestly higher resistance to tiamulin and virginiamycin M, residue 219 is a glycine, which we predict would not overlap with the PS_AL binding site (Lenart *et al.*, 2015). Thus, $VgaA_{LC}$ confers resistance to virginiamycin M and tiamulin despite the lack of overlap between the ARE ABCF and the antibiotic binding site (Table S2). For VgaL, the closest residue to the PS_AL binding site was Ala216, which had no predicted overlap with tiamulin, virginiamycin M, or lincomycin (Figure 4E). Strikingly, VgaL therefore confers resistance to lincomycin, virginiamycin M, and tiamulin without directly overlapping the binding sites of these antibiotics. In summary, there was no general pattern of overlap or non-overlap with the PS_AL binding sites among LsaA, $VgaA_{LC}$, and VgaL.

Mutational analysis of LsaA and $VgaA_{LC}$ ARDs

Our models of the ARD loops allowed us to design and test mutants for capacity to confer antibiotic resistance. When LsaA Phe257, which directly overlaps the PS_AL binding site (Figure 4C), was mutated to alanine, no change in resistance was observed (Figure S11). By contrast, mutation of Lys244, which is not situated close to the PS_AL binding sites but forms a hydrogen bond with 23S rRNA G2251 and G2252 of the P-loop (*Escherichia coli* numbering is used for 23S rRNA nucleotides), nearly abolished antibiotic resistance activity (Figure S11 and S12A–C). Combined, these observations indicate that LsaA does not confer resistance *via* simple steric occlusion, and that interactions with the P-loop may be required for positioning the LsaA ARD. For $VgaA_{LC}$, extensive alanine mutations within the ARD were

explored (Table S2). As expected from the above analyses and natural variants, mutating Val219—the only residue in $VgaA_{LC}$ that sterically overlaps the LS_AP binding site—did not affect the antibiotic resistance profile. Three residues at the beginning of α2, directly after the ARD loop, were required for resistance: Tyr223, which stacks with U2585 (part of the pleuromutilin and lincomycin binding sites); Phe224, which stacks with A2602 held in the center of the ARD; and Lys227, which forms a hydrogen bond with the 5′ phosphate of C2601 (Table S2). These residues do not overlap with the PS_AL binding site, but may be required to position the ARD in the PTC to impede antibiotic binding, or for the folding of the ARD itself (Figure S12D–F). In the naturally variable $VgaA_{LC}$ ARD, mutation of Ser213, which sits adjacent to U2506 and C2507 (Figure S12E), to alanine similarly reduced antibiotic resistance (Table S2). Of note, mutating the most conserved residue among VgaA variants in this region, Lys218, did not substantially affect resistance (Table S2) (Vimberg *et al*, 2020). Extensive alanine substitutions in the surrounding residues that contact the 23S rRNA (Figure S12D–F) either did not affect, or had only a mild influence on, the antibiotic resistance conferred by this protein (Table S2). In summary, mutation of $VgaA_{LC}$ residues that interact with 23S rRNA nucleotides that form part of the LS_AP binding pocket affected antibiotic-resistance activity.

Modulation of the ribosomal antibiotic binding site by ARE ABCFs

We next sought to explore how the ARDs of LsaA, $VgaA_{LC}$, and VgaL affect the conformation of the ribosomal PTC. The 23S rRNA A2602, which is flexible in the absence of tRNAs and positioned between the P- and A-tRNAs during peptidyl transfer, is bound and stabilized by all structurally characterized ARE ABCFs. In LsaA and VmlR, a tryptophan stacks and stabilizes A2602 in a flipped position (Figure S13) (Crowe-McAuliffe *et al.*, 2018). In $VgaA_{LC}$, VgaL, and MsrE, A2602 is instead positioned within the ARD loop, interacting with multiple residues from the ARE (Figure S13) (Su *et al.*, 2018). We have labelled five regions of domain V of the 23S rRNA, which form the PTC, PTC loops (PLs) 1–5 (Figure 5A) (Polacek & Mankin, 2005). There was a significant overlap between nucleotides that form the PS_AL binding pockets, nucleotides that were shifted when LsaA, $VgaA_{LC}$, or VgaL bound the 70S, and nucleotides known to be mutated or modified in antibiotic-resistant strains of bacteria (summarized in Figure 5A). Broadly, changes to the PTC were similar between the $VgaA_{LC}$- and VgaL-bound 70S structures, consistent with the grouping of these proteins together in the ARE1 subfamily (Figures 5E–G, S14, S15) (Murina *et al.*, 2019). Loop PL3, which contains nucleotides A2503 to U2506, was shifted upon binding of each ARE ABCF (Figure 5B–G). However, no residues from $VgaA_{LC}$ or VgaL directly contact PL3 (Figures 5E–G, S14

and S15). Rather, these ARE ABCFs directly displace PL2, which ordinarily positions PL3, perhaps thereby facilitating the distorted conformation of PL3 that is incompatible with antibiotic binding. In the $VgaA_{LC}$-bound state, U2585, which was poorly ordered in the LsaA- and VgaL-bound 70S, stacks with Tyr223 and would not be available to interact with tiamulin or virginiamycin M (Figure S14D–F). Substituting $VgaA_{LC}$ Tyr223 to alanine diminished antibiotic resistance, indicating that the reposition of U2585 contributes to antibiotic resistance conferred by this ARE ABCF (Table S2 and Figure S12F). 23S rRNA U2506 is additionally displaced in the $VgaA_{LC}$- and VgaL-bound 70S compared to the tiamulin- or lincomycin-bound 70S, potentially disrupting the binding site of these antibiotics (Figures S14A–C, S15A–C). By contrast, LsaA induced the most dramatic rearrangements in the PTC, with U2504 and G2505 in the LsaA-bound state predicted to strongly clash with each relevant antibiotic bound to the ribosome (Figure S5E–G and S16A–C). In the LsaA-bound ribosome, A2453 is shifted slightly away from the PTC and pairs with G2499 instead of U2500. This allows C2452, which normally pairs with U2504 to form part of the PS_AL binding pocket, to instead hydrogen-bond with U2500, thereby freeing U2504, and PL3 more generally, to reposition when LsaA is bound (Figure S16D, E).

Discussion

Model of antibiotic resistance mediated by LsaA, $VgaA_{LC}$, and VgaL

These observations allow us to propose a model for how ARE ABCFs confer antibiotic resistance to the host organism (Figure 6). PS_AL antibiotics have binding sites overlapping with the nascent polypeptide chain, and inhibit translation at, or soon after, initiation (Figure 6A) (Dornhelm & Högenauer, 1978; Meydan *et al.*, 2019; Orelle *et al.*, 2013). The incoming ARE ABCF binds in the E-site, triggering closure of the L1 stalk and inducing a distorted conformation of the P-tRNA. The ARD disrupts the antibiotic binding pocket in the PTC, causing drug release (Figure 6B). An incoming ternary complex delivers a tRNA to the A-site, which upon ARE ABCF egress and successful accommodation 'sweeps' the 3′ end of the P-tRNA into the PTC (Figure 6C, D). The trigger for nucleotide hydrolysis and exit of the ARE ABCF from the E site is unknown. We propose that rapid peptidyl transfer then creates a short nascent chain that overlaps with the antibiotic binding site, preventing re-binding of the PS_AL drug until the next round of translation (Figure 6D). Alternatively, an A-tRNA may partially accommodate on the stalled initiation complex prior to ARE ABCF binding, and become distorted as part of a 'knock-on' effect of P-tRNA disruption, consistent with the ability of ARE ABCFs to 'reset' the P-tRNA independently of additional accommodation events (Murina *et al.*, 2018). In this model, potentially only one round of ATP hydrolysis per translation cycle is necessary to confer resistance.

ARE ABCFs such as LsaA, $VgaA_{LC}$, VgaL, and VmlR confer resistance to PS_AL antibiotics but not phenicols or oxazolidinones (Sharkey & O'Neill, 2018). This observation has been puzzling, as both groups of antibiotics have overlapping binding sites (Dunkle *et al.*, 2010; Matzov *et al.*, 2017; Schlünzen *et al.*, 2004; Tu *et al.*, 2005; Wilson *et al.*, 2008). However, phenicols and oxazolidinones inhibit translation during elongation at specific motifs (Marks *et al*, 2016; Orelle *et al.*, 2013), while PS_AL antibiotics instead inhibit translation at the initiation stage (Dornhelm & Högenauer, 1978; Meydan *et al.*, 2019; Orelle *et al.*, 2013). The apparent specificity of LsaA, $VgaA_{LC}$, and VgaL for initiation complexes in our immunoprecipitations (Figure 2) matches the specificity of the antibiotics to which they confer resistance.

Do EQ_2-substituted ATPase-deficient variants of ARE ABCF, like the ones used in this study, bind the ribosome in the pre- or post-antibiotic-dissociation state (Figure 6B)? Although direct evidence is lacking, three reasons lead us to propose that these proteins are bound in the post-antibiotic-release state:

1) In the case of $VgaA_{LC}$ and VmlR the position of the ARD directly overlaps with the antibiotic binding site. Although the side chain of the overlapping amino acid is not

critical for antibiotic resistance in most instances, the overlap nonetheless implies mutually exclusive binding.

2) MsrE-EQ_2 stimulates dissociation of azithromycin from the ribosome (Su *et al.*, 2018).

3) Our attempts to form complexes containing both antibiotic and ARE ABCF have been unsuccessful, resulting in exclusive binding of either the ARE ABCF or the antibiotic, similarly to what we observed for TetM, a tetracycline-resistance ribosome protection protein (Arenz *et al*, 2015).

How does the ARE ABCF ARD mediate antibiotic resistance (Figure 6B, C)? In one model, by analogy to the TetM tetracycline resistance protein (Arenz *et al.*, 2015; Wilson *et al.*, 2020), the ARD may induce antibiotic dissociation by a direct steric overlap with the antibiotic. In the case of VmlR, substitutions of the Phe237 residue that overlaps the binding site of PS_AL antibiotics affect resistance to one of three relevant antibiotics, indicating that both direct steric overlap and an indirect, allosteric mechanism can contribute to resistance (Crowe-McAuliffe *et al.*, 2018). In the case of MsrE substitution of Leu242, which overlaps with the erythromycin binding site, as well as adjacent residues abolished or severely reduced the antibiotic resistance activity of this protein (Su *et al.*, 2018). In both cases, a mixture of direct steric overlap and allostery is consistent with the available data (Ero *et al.*, 2019). The ARDs of LsaA, $VgaA_{LC}$, and VgaL either do not directly overlap with the PS_AL binding site, or where there is an overlap, as with LsaA Phe257 and $VgaA_{LC}$ Val219, the side chains are not essential for resistance, implicating an allosteric mechanism for these proteins (Figures 4–5, S11, S12, Table S2). Alanine mutagenesis instead indicates that the side chains of residues surrounding the amino acid closest to the antibiotic-binding pocket, as well as those that contact the 23S rRNA, are necessary for resistance (Figures S11, S12 and Table S2). These residues may position the ARD in the PTC. No single set of 23S rRNA rearrangements was identical among LsaA, $VgaA_{LC}$, and VgaL, although displacement of PTC loop PL3, especially residue U2504, was ultimately observed in each ARE ABCF–70S structure (Figure 5).

In summary, we present three new structures of ARE ABCFs bound to 70S ribosomes from relevant Gram-positive pathogenic bacteria and present the first model of the ribosome from *Listeria monocytogenes*. Our structures and mutagenesis experiments support an allosteric mechanism of ARE ABCF action, and hint at a rationalization for the specificity of LsaA, $VgaA_{LC}$, and VgaL for PS_AL antibiotics. Each ARE ABCF binds the 70S similarly as observed for other bacterial ABCF proteins, but alters the geometry of the PTC distinctively, consistent with the convergent evolution—and divergent sequences—of this class of ABCF proteins.

Acknowledgments

We are grateful to Barbara E. Murray for sharing *E. faecalis* Δ*lsaA* (*lsa*::Kan) strain TX5332 (Singh *et al.*, 2002), Jose A. Lemos for sharing $pCIE_{cam}$ plasmid vector (Weaver *et al*, 2017). We thank Michael Hall for help with cryo-EM data collection. The electron microscopy data was collected at the Umeå Core Facility for Electron Microscopy, a node of the Cryo-EM Swedish National Facility, funded by the Knut and Alice Wallenberg, Family Erling Persson and Kempe Foundations, SciLifeLab, Stockholm University and Umeå University. This work was supported by the Deutsche Forschungsgemeinschaft (DFG) (grant WI3285/8-1 to D.N.W), the Swedish Research Council (Vetenskapsrådet) grants (2017-03783 to V.H. and 2019-01085 to G.C.A.), Ragnar Söderbergs Stiftelse (to V.H.), postdoctoral grant from the Umeå Centre for Microbial Research, UCMR (to H.T.), the European Union from the European Regional Development Fund through the Centre of Excellence in Molecular Cell Engineering (2014-2020.4.01.15-0013 to V.H.); and the Estonian Research Council (PRG335 to V.H.). D.N.W. and V.H. groups are also supported by the Deutsche Zentrum für Luft- und Raumfahrt (DLR01KI1820 to D.N.W.) and the Swedish Research Council (2018-00956 to V.H.) within the RIBOTARGET consortium under the framework of JPIAMR.

Figures

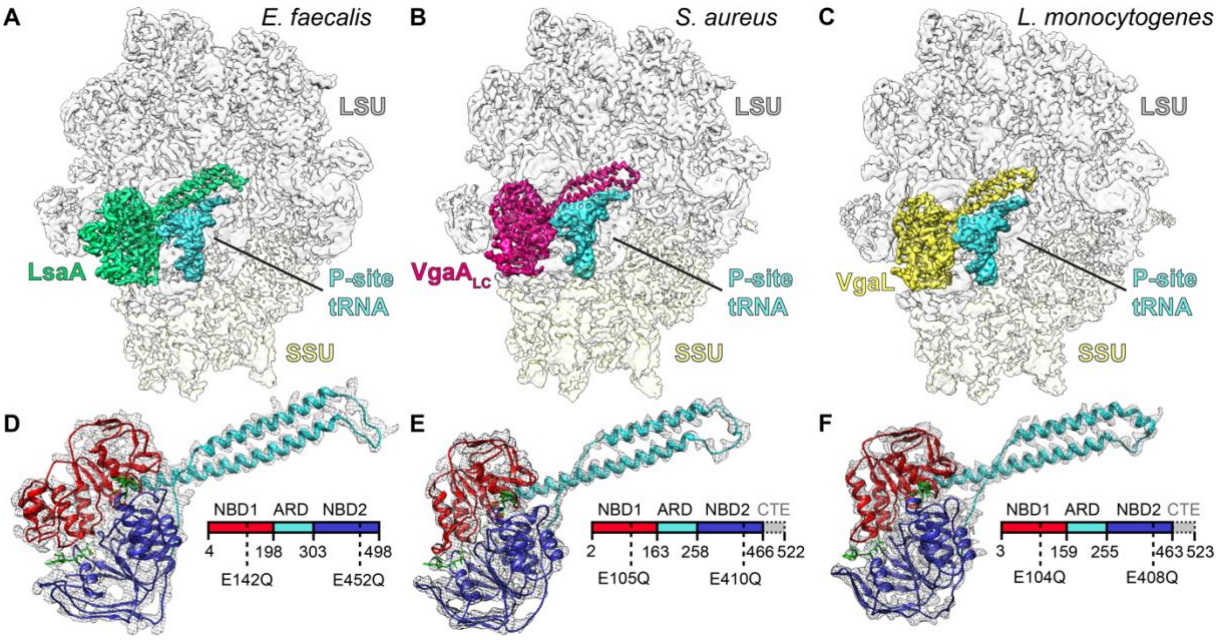

Fig. 1 Cryo-EM structures of ARE ABCF–ribosome complexes. (**A–C**) Cryo-EM maps with isolated densities for (**A**) *E. faecalis* LsaA (green), (**B**) *S. aureus* $VgaA_{LC}$ (magenta), (**C**) *L. monocytogenes* VgaL (yellow) as well as P-site tRNA (cyan), small subunit (SSU, yellow) and large subunit (LSU, grey). (**D–F**) Density (grey mesh) with molecular model for (**D**) LsaA, (**E**) $VgaA_{LC}$, and (**F**) VgaL, coloured according to domain as represented in the associated schematics: nucleotide binding domain 1 (NBD1, red), antibiotic-resistance domain (ARD, cyan), nucleotide binding domain 2 (NBD2, blue) and C-terminal extension (CTE, grey, not modelled). In (**D–F**), the ATP nucleotides are coloured green.

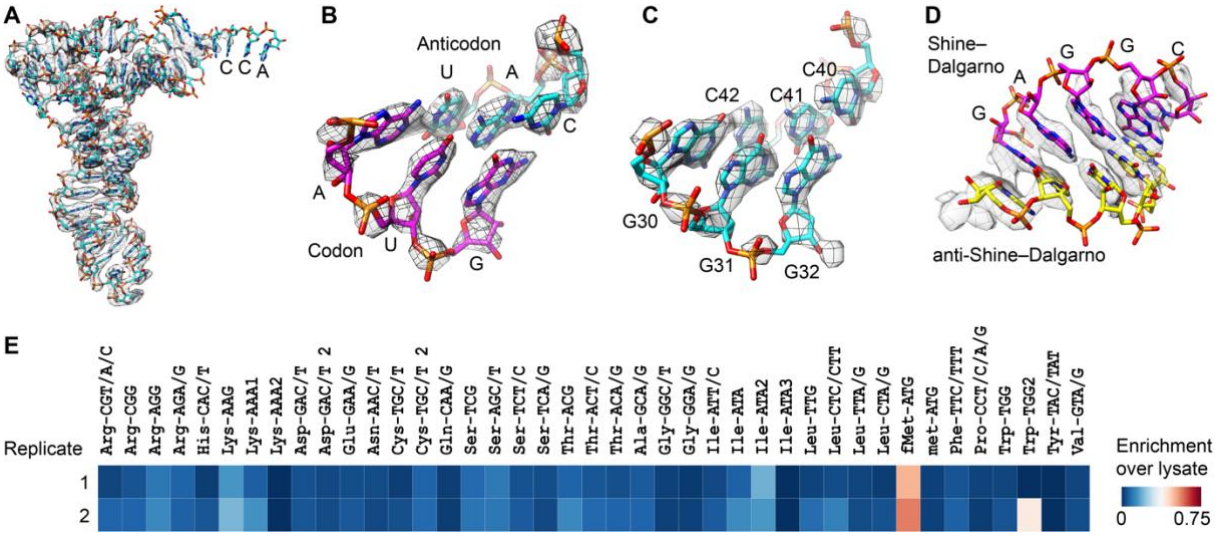

Figure 2. The LsaA–70S complex contains an initiator tRNA and SD-helix. (**A–D**) Isolated density (grey mesh) with molecular models (sticks) for (**A**) initiator $tRNA^{fMet}$ (cyan), (**B**) interaction between AUG start codon of the mRNA (magenta) and anticodon of initiator $tRNA^{fMet}$ (cyan) in the P-site, (**C**) three G-C base pairs specific to the initiator $tRNA^{fMet}$ (cyan), and (**D**) helix formed between Shine-Dalgarno (SD) sequence of the mRNA (magenta) and anti-SD of the 16S rRNA (yellow). (**E**) Replicate tRNA microarray analysis of the LsaA–70S complex, illustrating the enrichment of initiator $tRNA^{fMet}$ in the LsaA–70S complex over the lysate. Confidence intervals between replicates were 92%.

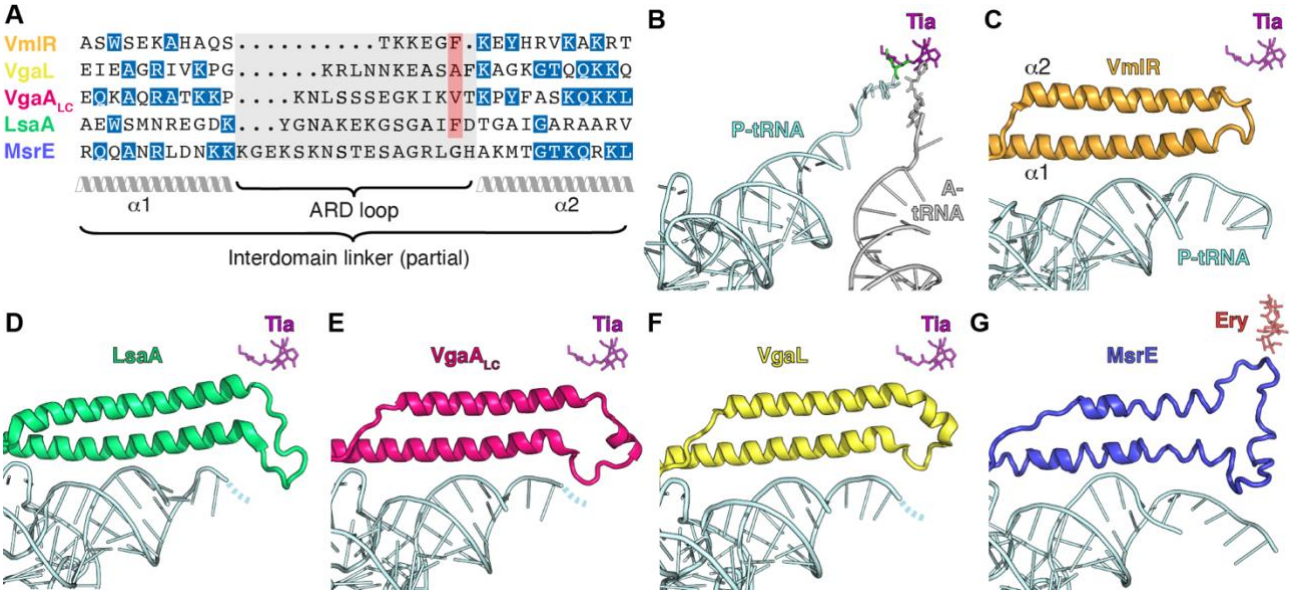

Fig. 3. Comparison of the ARD loops of different ARE ABCFs. (**A**) The sequence length of the ARD loops differs significantly for VmlR, VgaL, $VgaA_{LC}$, LsaA and MsrE. Although the lack of sequence homology precludes accurate sequence alignment of the ARD loops, the red highlighted residues can be aligned structurally. (**B–G**) Comparison of the positions of (**B**) A-site tRNA (grey) and P-site tRNA (cyan) from pre-attack state (PDB 1VY4) (Polikanov *et al*, 2014), with shifted P-site tRNA (cyan) and ABCF ARD from ribosome complexes containing (**C**) VmlR (orange, PDB 6HA8) (Crowe-McAuliffe *et al.*, 2018), (**D**) LsaA (green), (**E**) $VgaA_{LC}$ (magenta), (**F**) VgaL (yellow), and (**G**) MsrE (blue, PDB 5ZLU) (Su *et al.*, 2018). In (**B–G**), the relative position of either tiamulin (Tia, magenta, PDB 1XBP) (Schlünzen *et al.*, 2004) or erythromycin (Ery, red, PDB 4V7U) (Dunkle *et al.*, 2010) has been superimposed.

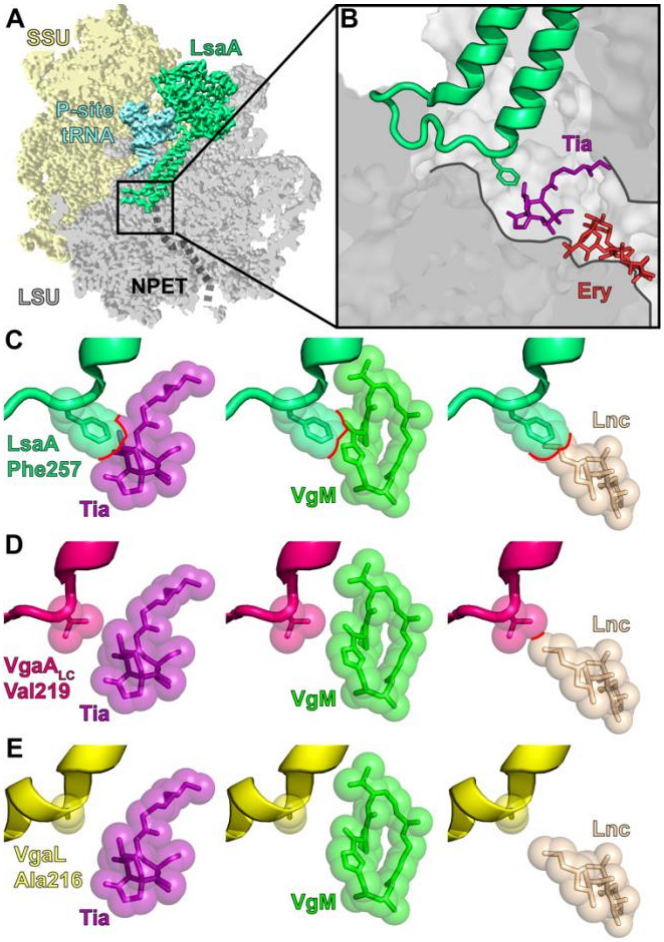

Fig. 4 Interaction of LsaA, VgaA$_{LC}$ and VgaL at the peptidyltransferase centre. (**A–B**) LsaA and distorted P-site tRNA superimposed on a transverse section of the large subunit (LSU, grey) to reveal (**A**) the ARD of LsaA extending into the nascent polypeptide exit tunnel (NPET) and (**B**) the relative position of Phe257 of LsaA to tiamulin (Tia, purple, PDB 1XBP) (Schlünzen *et al.*, 2004) and erythromycin (Ery, red, PDB 4V7U) (Dunkle *et al.*, 2010). (**C–E**) Relative position of LsaA (green, row **C**), VgaA$_{LC}$ (pink, row **D**) and VgaL (yellow, row **E**) to tiamulin (Tia, purple, PDB 1XBP), virginiamycin M (VgM, lime, PDB 1YIT) (Tu *et al.*, 2005), lincomycin (Lnc, tan, PDB 5HKV) (Matzov *et al.*, 2017). Clashes in **C–E** are shown with red outlines.

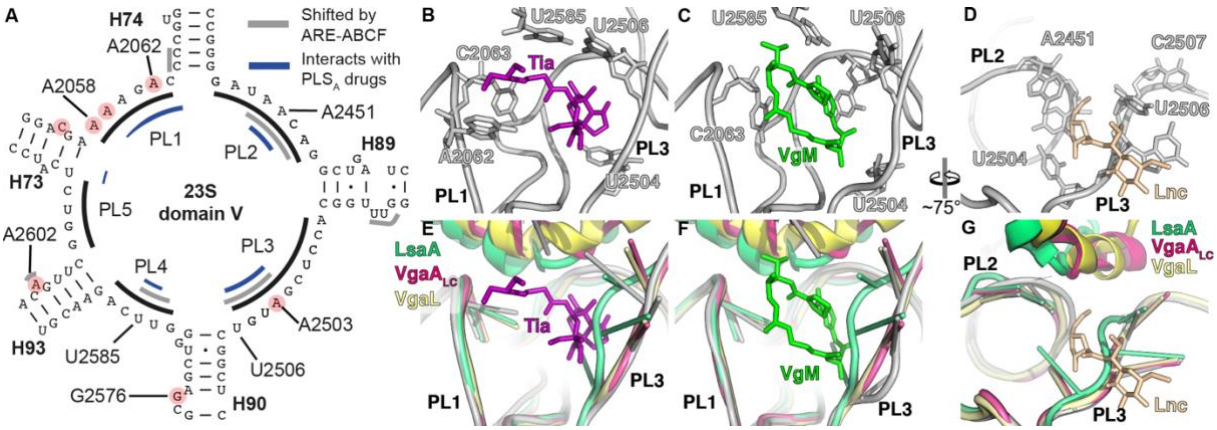

Fig. 5 ARE ABCF binding induces allosteric conformational changes at the PTC. (**A**) Secondary structure of peptidyltransferase ring within domain V of the 23S rRNA, highlighting residues within PTC loops 1–4 (PL1–4) that (i) comprise the binding site of PS$_A$L antibiotics (blue), (ii) undergo conformational changes upon ARE ABCF binding (grey) and (iii) confer resistance to PS$_A$L antibiotics (red circles). (**B–D**) Binding site of (**B**) tiamulin (Tia, magenta, PDB 1XBP; (Schlünzen *et al.*, 2004), (**C**) virginiamycin M (VgM, lime, PDB YIT; (Tu *et al.*, 2005) and (**D**) lincomycin (Lnc, tan, PDB 5HKV) (Matzov *et al.*, 2017) on the ribosome. (**E–G**) Comparison of conformations of rRNA nucleotides comprising the (**E**) Tia, (**F**) VgM and (**G**) Lnc binding site (shown as grey cartoon ladder representation), with rRNA conformations when LsaA (green), VgaA$_{LC}$ (magenta) or VgaL (yellow) are bound.

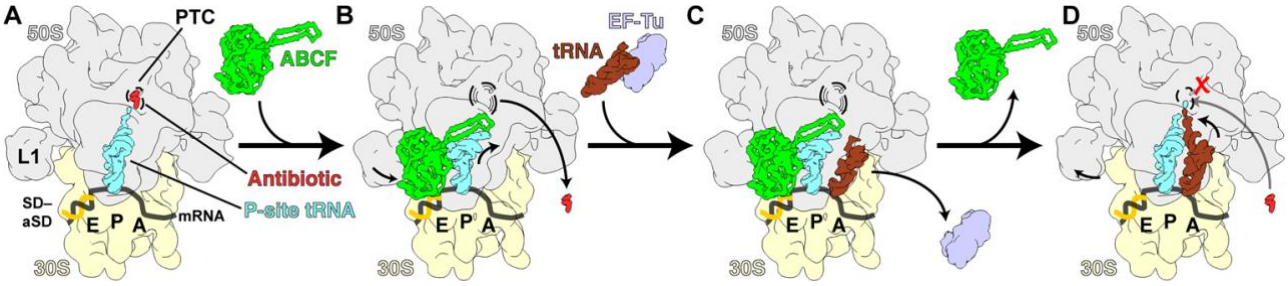

Fig. 6 Model for ribosome protection by ARE ABCFs VmlR, LsaA, VgaA$_{LC}$ and VgaL. (**A**) PS$_A$L-stalled ribosomes containing an initiator-tRNA in the P-site are recognized by the ARE ABCFs such as VmlR, LsaA, VgaA$_{LC}$ and VgaL, which bind to the E-site of the ribosome with a closed ATP-bound conformation. (**B**) Binding of the ARE ABCF induces a shifted P-site tRNA conformation in the ribosome allowing the ARD of the ARE ABCF to access the peptidyl-transferase center (PTC). The ARD induces conformational changes within the 23S rRNA at the PTC that promotes dissociation of the drug from its binding site (shown as dashed lines). (**C**) aminoacyl- tRNAs can still bind to the ARE ABCF-bound ribosomal complex, but cannot accommodate at the PTC due to the presence of the ABCF and shifted P-site tRNA conformation. (**D**) Hydrolysis of ATP to ADP leads to dissociation of ARE ABCF from the ribosome, which may allow the peptidyl-tRNA as well as the incoming aminoacyl- tRNA to simultaneously accommodate at the PTC. Peptide bond formation can then ensue, converting the ribosome from an initiation to an elongation (pre-translocation) state, which is resistant to the action of initiation inhibitors, such as PS$_A$L antibiotics.

References

Allignet J, Loncle V, El Solh N (1992) Sequence of a staphylococcal plasmid gene, *vga*, encoding a putative ATP-binding protein involved in resistance to virginiamycin A-like antibiotics. *Gene* 117: 45-51

Andersen CBF, Becker T, Blau M, Anand M, Halic M, Balar B, Mielke T, Boesen T, Pedersen JS, Spahn CMT *et al* (2006) Structure of eEF3 and the mechanism of transfer RNA release from the E-site. *Nature* 443: 663-668

Antonelli A, D'Andrea MM, Brenciani A, Galeotti CL, Morroni G, Pollini S, Varaldo PE, Rossolini GM (2018) Characterization of poxtA, a novel phenicol–oxazolidinone–tetracycline resistance gene from an MRSA of clinical origin. *J Antimicrob Chemother* 73: 1763-1769

Arenz S, Nguyen F, Beckmann R, Wilson DN (2015) Cryo-EM structure of the tetracycline resistance protein TetM in complex with a translating ribosome at 3.9-Å resolution. *Proc Natl Acad Sci U S A* 112: 5401-5406

Arnaud M, Chastanet A, Débarbouillé M (2004) New vector for efficient allelic replacement in naturally nontransformable, low-GC-content, gram-positive bacteria. *Appl Environ Microbiol* 70: 6887-6891

Becker T, Franckenberg S, Wickles S, Shoemaker CJ, Anger AM, Armache J-P, Sieber H, Ungewickell C, Berninghausen O, Daberkow I (2012) Structural basis of highly conserved ribosome recycling in eukaryotes and archaea. *Nature* 482: 501-506

Bhardwaj P, Ziegler E, Palmer KL (2016) Chlorhexidine induces VanA-type vancomycin resistance genes in enterococci. *Antimicrobial agents and chemotherapy* 60: 2209-2221

Camargo AC, Woodward JJ, Nero LA (2016) The continuous challenge of characterizing the foodborne pathogen *Listeria monocytogenes*. *Foodborne Pathog Dis* 13: 405-416

Candiano G, Bruschi M, Musante L, Santucci L, Ghiggeri GM, Carnemolla B, Orecchia P, Zardi L, Righetti PG (2004) Blue silver: a very sensitive colloidal Coomassie G-250 staining for proteome analysis. *Electrophoresis* 25: 1327-1333

Casañal A, Lohkamp B, Emsley P (2020) Current developments in *Coot* for macromolecular model building of electron cryo-microscopy and crystallographic data. *Protein Sci* 29: 1069-1078

Chen B, Boël G, Hashem Y, Ning W, Fei J, Wang C, Gonzalez RL, Hunt JF, Frank J (2014) EttA regulates translation by binding the ribosomal E site and restricting ribosome-tRNA dynamics. *Nat Struct Mol Biol* 21: 152-159

Chesneau O, Ligeret H, Hosan-Aghaie N, Morvan A, Dassa E (2005) Molecular analysis of resistance to streptogramin A compounds conferred by the Vga proteins of Staphylococci. *Antimicrob Agents Chemother* 49: 973-980

Corrigan RM, Foster TJ (2009) An improved tetracycline-inducible expression vector for *Staphylococcus aureus*. *Plasmid* 61: 126-129

530 Crowe-McAuliffe C, Graf M, Huter P, Takada H, Abdelshahid M, Nováček J, Murina V,
531 Atkinson GC, Hauryliuk V, Wilson DN (2018) Structural basis for antibiotic resistance
532 mediated by the *Bacillus subtilis* ABCF ATPase VmlR. *Proc Natl Acad Sci U S A* 115: 8978-
533 8983
534 Dar D, Shamir M, Mellin JR, Koutero M, Stern-Ginossar N, Cossart P, Sorek R (2016) Term-
535 seq reveals abundant ribo-regulation of antibiotics resistance in bacteria. *Science* 352: 9822-
536 9822
537 Davidson AL, Dassa E, Orelle C, Chen J (2008) Structure, function, and evolution of bacterial
538 ATP-binding cassette systems. *Microbiol Mol Biol Rev* 72: 317-364
539 Davis Dv, McAlpine JB, Pazoles CJ, Talbot MK, Alder EA, White AC, Jonas BM, Murray BE,
540 Weinstock GM, Rogers BL (2001) *Enterococcus faecalis* multi-drug resistance transporters:
541 application for antibiotic discovery. *J Mol Microbiol Biotechnol* 3: 179-184
542 Dornhelm P, Högenauer G (1978) The effects of tiamulin, a semisynthetic pleuromutilin
543 derivative, on bacterial polypeptide chain initiation. *Eur J Biochem* 91: 465-473
544 Dorrian J, Kerr I (2009) *Can ABC proteins confer drug resistance in micro-organisms without*
545 *being export pumps?* Caister Academic Press
546 Dunkle JA, Xiong L, Mankin AS, Cate JH (2010) Structures of the *Escherichia coli* ribosome
547 with antibiotics bound near the peptidyl transferase center explain spectra of drug action.
548 *Proc Natl Acad Sci U S A* 107: 17152-17157
549 Duval M, Dar D, Carvalho F, Rocha EP, Sorek R, Cossart P (2018) HflXr, a homolog of a
550 ribosome-splitting factor, mediates antibiotic resistance. *Proc Natl Acad Sci U S A* 115:
551 13359-13364
552 Ero R, Kumar V, Su W, Gao YG (2019) Ribosome protection by ABC-F proteins—Molecular
553 mechanism and potential drug design. *Protein Sci* 28: 684-693
554 Fairweather N, Kennedy S, Foster T, Kehoe M, Dougan G (1983) Expression of a cloned
555 *Staphylococcus aureus* α-hemolysin determinant in *Bacillus subtilis* and *Staphylococcus*
556 *aureus*. *Infect Immun* 41: 1112-1117
557 Fischer N, Neumann P, Konevega AL, Bock LV, Ficner R, Rodnina MV, Stark H (2015)
558 Structure of the *E. coli* ribosome–EF-Tu complex at < 3 Å resolution by Cs-corrected cryo-
559 EM. *Nature* 520: 567-570
560 Fostier CR, Monlezun L, Ousalem F, Singh S, Hunt JF, Boël G (2020) ABC-F translation
561 factors: from antibiotic resistance to immune response. *FEBS Lett*
562 Freitas AR, Elghaieb H, León-Sampedro R, Abbassi MS, Novais C, Coque TM, Hassen A,
563 Peixe L (2017) Detection of *optrA* in the African continent (Tunisia) within a mosaic
564 *Enterococcus faecalis* plasmid from urban wastewaters. *J Antimicrob Chemother* 72: 3245-
565 3251

Gabdulkhakov A, Tishchenko S, Mikhaylina A, Garber M, Nevskaya N, Nikonov S (2017) Crystal Structure of the 23S rRNA Fragment Specific to r-Protein L1 and Designed Model of the Ribosomal L1 Stalk from Haloarcula marismortui. *Crystals* 7: 37

Gerovac M, Tampé R (2019) Control of mRNA translation by versatile ATP-driven machines. *Trends Biochem Sci* 44: 167-180

Glaser P, Frangeul L, Buchrieser C, Rusniok C, Amend A, Baquero F, Berche P, Bloecker H, Brandt P, Chakraborty T (2001) Comparative genomics of *Listeria* species. *Science* 294: 849-852

Golubev A, Fatkhullin B, Khusainov I, Jenner L, Gabdulkhakov A, Validov S, Yusupova G, Yusupov M, Usachev K (2020) Cryo-EM structure of the ribosome functional complex of the human pathogen *Staphylococcus aureus* at 3.2 Å resolution. *FEBS letters*

Henderson R, Sali A, Baker ML, Carragher B, Devkota B, Downing KH, Egelman EH, Feng Z, Frank J, Grigorieff N (2012) Outcome of the first electron microscopy validation task force meeting. *Structure* 20: 205-214

Heuer A, Gerovac M, Schmidt C, Trowitzsch S, Preis A, Kötter P, Berninghausen O, Becker T, Beckmann R, Tampe R (2017) Structure of the 40S–ABCE1 post-splitting complex in ribosome recycling and translation initiation. *Nat Struct Mol Biol* 24: 453-460

Ho SN, Hunt HD, Horton RM, Pullen JK, Pease LR (1989) Site-directed mutagenesis by overlap extension using the polymerase chain reaction. *Gene* 77: 51-59

Horsburgh MJ, Aish JL, White IJ, Shaw L, Lithgow JK, Foster SJ (2002) σB modulates virulence determinant expression and stress resistance: characterization of a functional rsbU strain derived from *Staphylococcus aureus* 8325-4. *J Bacteriol* 184: 5457-5467

Hot C, Berthet N, Chesneau O (2014) Characterization of *sal*(A), a novel gene responsible for lincosamide and ttreptogramin A resistance in *Staphylococcus sciuri*. *Antimicrob Agents Chemother* 58: 3335-3341

Iimura M, Hayashi W, Arai E, Natori T, Horiuchi K, Matsumoto G, Tanaka H, Soga E, Nagano Y, Arakawa Y (2020) Identification of a multiresistant mosaic plasmid carrying a new segment of *IS1216E*-flanked *optrA* with integrated Tn551-*ermB* element in linezolid-resistant *Enterococcus faecalis* human isolate. *J Glob Antimicrob Res* 22: 679-699

Jacquet E, Girard JM, Ramaen O, Pamlard O, Lévaique H, Betton JM, Dassa E, Chesneau O (2008) ATP hydrolysis and pristinamycin IIA inhibition of the *Staphylococcus aureus* Vga(A), a dual ABC protein involved in streptogramin A resistance. *J Biol Chem* 283: 25332-25339

James NR, Brown A, Gordiyenko Y, Ramakrishnan V (2016) Translational termination without a stop codon. *Science* 354: 1437-1440

Johnson ZL, Chen J (2018) ATP binding enables substrate release from Multidrug Resistance Protein 1. *Cell* 172: 81-89

603 Khusainov I, Vicens Q, Bochler A, Grosse F, Myasnikov A, Ménétret J-F, Chicher J, Marzi S,
604 Romby P, Yusupova G (2016) Structure of the 70S ribosome from human pathogen
605 *Staphylococcus aureus*. *Nucleic Acids Res* 44: 10491-10504
606 Koberska M, Vesela L, Vimberg V, Lenart J, Vesela J, Kamenik Z, Janata J, Novotna GB
607 (2020) Beyond self-resistance: ABCF ATPase LmrC is a signal-transducing component of an
608 antibiotic-driven signaling cascade hastening the onset of lincomycin biosynthesis. *bioRxiv*:
609 2020.2010.2016.343517
610 Krishnan A, Burroughs AM, Iyer LM, Aravind L (2020) Comprehensive classification of ABC
611 ATPases and their functional radiation in nucleoprotein dynamics and biological conflict
612 systems. *Nucleic Acids Res* 48: 10045–10075
613 Kucukelbir A, Sigworth FJ, Tagare HD (2014) Quantifying the local resolution of cryo-EM
614 density maps. *Nat Methods* 11: 63-65
615 Lenart J, Vimberg V, Vesela L, Janata J, Novotna GB (2015) Detailed mutational analysis of
616 Vga(A) interdomain linker: Implication for antibiotic resistance specificity and mechanism.
617 *Antimicrob Agents Chemother* 59: 1360-1364
618 Liebschner D, Afonine PV, Baker ML, Bunkóczi G, Chen VB, Croll TI, Hintze B, Hung L-W,
619 Jain S, McCoy AJ (2019) Macromolecular structure determination using X-rays, neutrons and
620 electrons: recent developments in Phenix. *Acta Crystallogr D Struct Biol* 75: 861-877
621 Loveland AB, Demo G, Grigorieff N, Korostelev AA (2017) Ensemble cryo-EM elucidates the
622 mechanism of translation fidelity. *Nature* 546: 113-117
623 Magill SS, Edwards JR, Bamberg W, Beldavs ZG, Dumyati G, Kainer MA, Lynfield R,
624 Maloney M, McAllister-Hollod L, Nadle J (2014) Multistate point-prevalence survey of health
625 care-associated infections. *N Engl J Med* 370: 1198-1208
626 Mamtora D, Saseedharan S, Bhalekar P, Katakdhond S (2019) Microbiological profile and
627 antibiotic susceptibility pattern of Gram-positive isolates at a tertiary care hospital. *J Lab*
628 *Physicians* 11: 144-148
629 Marks J, Kannan K, Roncase EJ, Klepacki D, Kefi A, Orelle C, Vazquez-Laslop N, Mankin
630 AS (2016) Context-specific inhibition of translation by ribosomal antibiotics targeting the
631 peptidyl transferase center. *Proc Natl Acad Sci U S A* 113: 12150-12155
632 Matzov D, Eyal Z, Benhamou RI, Shalev-Benami M, Halfon Y, Krupkin M, Zimmerman E,
633 Rozenberg H, Bashan A, Fridman M (2017) Structural insights of lincosamides targeting the
634 ribosome of *Staphylococcus aureus*. *Nucleic Acids Res* 45: 10284-10292
635 Mendes RE, Paukner S, Doyle TB, Gelone SP, Flamm RK, Sader HS (2019) Low
636 Prevalence of Gram-positive isolates showing elevated lefamulin MIC results during the
637 SENTRY Surveillance Program for 2015–2016 and characterization of resistance
638 mechanisms. *Antimicrob Agents Chemother* 63: e02158-02118

639 Meydan S, Marks J, Klepacki D, Sharma V, Baranov PV, Firth AE, Margus T, Kefi A,
640 Vázquez-Laslop N, Mankin AS (2019) Retapamulin-assisted ribosome profiling reveals the
641 alternative bacterial proteome. *Mol Cell* 74: 481-493
642 Monk IR, Gahan CG, Hill C (2008) Tools for functional postgenomic analysis of *Listeria*
643 *monocytogenes*. *Appl Environ Microbiol* 74: 3921-3934
644 Moriya T, Saur M, Stabrin M, Merino F, Voicu H, Huang Z, Penczek PA, Raunser S,
645 Gatsogiannis C (2017) High-resolution single particle analysis from electron cryo-microscopy
646 images using SPHIRE. *J Vis Exp*: e55448
647 Murina V, Kasari M, Hauryliuk V, Atkinson GC (2018) Antibiotic resistance ABCF proteins
648 reset the peptidyl transferase centre of the ribosome to counter translational arrest. *Nucleic*
649 *Acids Res*: 1-11
650 Murina V, Kasari M, Takada H, Hinnu M, Saha CK, Grimshaw JW, Seki T, Reith M, Putrinš
651 M, Tenson T (2019) ABCF ATPases involved in protein synthesis, ribosome assembly and
652 antibiotic resistance: structural and functional diversification across the tree of life. *J Mol Biol*
653 431: 3568-3590
654 Murphy EL, Singh KV, Avila B, Kleffmann T, Gregory ST, Murray BE, Krause KL, Khayat R,
655 Jogl G (2020) Cryo-electron microscopy structure of the 70S ribosome from *Enterococcus*
656 *faecalis*. *Sci Rep* 10: 16301
657 Noeske J, Wasserman MR, Terry DS, Altman RB, Blanchard SC, Cate JH (2015) High-
658 resolution structure of the *Escherichia coli* ribosome. *Nat Struct Mol Biol* 22: 336-341
659 Novotna G, Janata J (2006) A new evolutionary variant of the streptogramin A resistance
660 protein, Vga(A)$_{LC}$, from *Staphylococcus haemolyticus* with shifted substrate specificity
661 towards lincosamides. *Antimicrob Agent Chemother* 50: 4070-4076
662 Ohki R, Tateno K, Takizawa T, Aiso T, Murata M (2005) Transcriptional termination control of
663 a novel ABC transporter gene involved in antibiotic resistance in *Bacillus subtilis*. *J Bacteriol*
664 187: 5946-5954
665 Orelle C, Carlson S, Kaushal B, Almutairi MM, Liu H, Ochabowicz A, Quan S, Pham VC,
666 Squires CL, Murphy BT (2013) Tools for characterizing bacterial protein synthesis inhibitors.
667 *Antimicrob Agent Chemother* 57: 5994-6004
668 Ousalem F, Singh S, Chesneau O, Hunt JF, Boël G (2019) ABC-F proteins in mRNA
669 translation and antibiotic resistance. *Res Microbiol* 170: 435-447
670 O'Neill A (2010) *Staphylococcus aureus* SH1000 and 8325-4: comparative genome
671 sequences of key laboratory strains in staphylococcal research. *Letters in applied*
672 *microbiology* 51: 358-361
673 Pettersen EF, Goddard TD, Huang CC, Couch GS, Greenblatt DM, Meng EC, Ferrin TE
674 (2004) UCSF Chimera—a visualization system for exploratory research and analysis. *J*
675 *Comp Chem* 25: 1605-1612

676 Pfaller MA, Cormican M, Flamm RK, Mendes RE, Jones RN, 2019. Temporal and
677 geographic variation in antimicrobial susceptibility and resistance patterns of enterococci:
678 results from the SENTRY Antimicrobial Surveillance Program, 1997-2016, Open Forum
679 Infect Dis. Oxford University Press US, pp. S54-S62.
680 Polacek N, Mankin AS (2005) The ribosomal peptidyl transferase center: structure, function,
681 evolution, inhibition. *Crit Rev Biochem Mol Biol* 40: 285-311
682 Polikanov YS, Starosta AL, Juette MF, Altman RB, Terry DS, Lu W, Burnett BJ, Dinos G,
683 Reynolds KA, Blanchard SC *et al* (2015) Distinct tRNA accommodation intermediates
684 observed on the ribosome with the antibiotics Hygromycin A and A201A. *Mol Cell* 58: 832-
685 844
686 Polikanov YS, Steitz TA, Innis CA (2014) A proton wire to couple aminoacyl-tRNA
687 accommodation and peptide-bond formation on the ribosome. *Nat Struct Mol Biol* 21: 787-
688 793
689 Pulk A, Cate JH (2013) Control of ribosomal subunit rotation by elongation factor G. *Science*
690 340: 1-7
691 Ranjan N, Pochopien AA, Wu CC-C, Beckert B, Blanchet S, Green R, Rodnina MV, Wilson
692 DN (2020) eEF3 promotes late stages of tRNA translocation on the ribosome. *bioRxiv*
693 Rees DC, Johnson E, Lewinson O (2009) ABC transporters: the power to change. *Nat Rev*
694 *Mol Cell Biol* 10: 218-227
695 Reynolds ED, Cove JH (2005) Resistance to telithromycin is conferred by *msr*(A), *msrC* and
696 *msr*(D) in *Staphylococcus aureus*. *J Antimicrob Chemother* 56: 1179-1180
697 Rohou A, Grigorieff N (2015) CTFFIND4: Fast and accurate defocus estimation from electron
698 micrographs. *J Struct Biol* 192: 216-221
699 Ross JI, Eady EA, Cove JH, Cunliffe WJ, Baumberg S, Wootton JC (1990) Inducible
700 erythromycin resistance in staphlyococci is encoded by a member of the ATP-binding
701 transport super-gene family. *Mol Microbiol* 4: 1207-1214
702 Ross JI, Farrell AM, Eady EA, Cove JH, Cunliffe WJ (1989) Characterisation and molecular
703 cloning of the novel macrolide-streptogramin B resistance determinant from *Staphylococcus*
704 *epidermidis*. *J Antimicrob Chemother* 24: 851-862
705 Rozov A, Khusainov I, El Omari K, Duman R, Mykhaylyk V, Yusupov M, Westhof E, Wagner
706 A, Yusupova G (2019) Importance of potassium ions for ribosome structure and function
707 revealed by long-wavelength X-ray diffraction. *Nat Commun* 10: 1-12
708 Sadowy E (2018) Linezolid resistance genes and genetic elements enhancing their
709 dissemination in enterococci and streptococci. *Plasmid* 99: 89-98
710 Schenk S, Laddaga RA (1992) Improved method for electroporation of *Staphylococcus*
711 *aureus*. *FEMS Microbiol Lett* 94: 133-138

712 Scheres SH, Chen S (2012) Prevention of overfitting in cryo-EM structure determination. *Nat*
713 *Methods* 9: 853-854
714 Schlünzen F, Pyetan E, Fucini P, Yonath A, Harms JM (2004) Inhibition of peptide bond
715 formation by pleuromutilins: the structure of the 50S ribosomal subunit from *Deinococcus*
716 *radiodurans* in complex with tiamulin. *Mol Microbiol* 54: 1287-1294
717 Sharkey LK, Edwards TA, O'Neill AJ (2016) ABC-F proteins pediate antibiotic resistance
718 through ribosomal protection. *mBio* 7: e01975
719 Sharkey LK, O'Neill AJ (2018) Antibiotic resistance ABC-F proteins: bringing target protection
720 into the limelight. *ACS Infect Dis* 4: 239-246
721 Simon R, Priefer U, Pühler A (1983) A broad host range mobilization system for *in vivo*
722 genetic engineering: transposon mutagenesis in Gram negative bacteria. *Bio/technology* 1:
723 784-791
724 Singh KV, Malathum K, Murray BE (2001) Disruption of an *Enterococcus faecium* species-
725 specific gene, a homologue of acquired macrolide resistance genes of staphylococci, is
726 associated with an increase in macrolide susceptibility. *Antimicrob Agent Chemother* 45:
727 263-266
728 Singh KV, Weinstock GM, Murray BE (2002) An *Enterococcus faecalis* ABC homologue
729 (Lsa) is required for the resistance of this species to clindamycin and quinupristin-dalfopristin.
730 *Antimicrob Agents Chemother* 46: 1845-1850
731 Su W, Kumar V, Ding Y, Ero R, Serra A, Lee BST, Wong ASW, Shi J, Sze SK, Yang L
732 (2018) Ribosome protection by antibiotic resistance ATP-binding cassette protein. *Proc Natl*
733 *Acad Sci U S A* 115: 5157-5162
734 Takada H, Roghanian M, Murina V, Dzhygyr I, Murayama R, Akanuma G, Atkinson GC,
735 Garcia-Pino A, Hauryliuk V (2020) The C-terminal RRM/ACT domain is crucial for fine-tuning
736 the activation of 'long' RelA-SpoT Homolog enzymes by ribosomal complexes. *Front*
737 *Microbiol* 11: 277
738 Thomas C, Tampé R (2020) Structural and mechanistic principles of ABC transporters. *Ann*
739 *Rev Biochem* 89: 605-636
740 Tishchenko S, Gabdulkhakov A, Nevskaya N, Sarskikh A, Kostareva O, Nikonova E,
741 Sycheva A, Moshkovskii S, Garber M, Nikonov S (2012) High-resolution crystal structure of
742 the isolated ribosomal L1 stalk. *Acta Crystallogr D Biol Crystallogr* 68: 1051-1057
743 Tu D, Blaha G, Moore PB, Steitz TA (2005) Structures of MLS_BK antibiotics bound to
744 mutated large ribosomal subunits provide a structural explanation for resistance. *Cell* 121:
745 257-270
746 Vimberg V, Cavanagh JP, Novotna M, Lenart J, Nguyen Thi Ngoc B, Vesela J, Pain M,
747 Koberska M, Balikova Novotna G (2020) Ribosome-mediated attenuation of *vga*(A)

748 expression is shaped by the antibiotic resistance specificity of Vga(A) protein variants.
749 *Antimicrob Agent Chemother* 64: e00666-00620
750 Voorhees RM, Schmeing TM, Kelley AC, Ramakrishnan V (2010) The mechanism for
751 activation of GTP hydrolysis on the ribosome. *Science* 330: 835-838
752 Wang Y, Lv Y, Cai J, Schwarz S, Cui L, Hu Z, Zhang R, Li J, Zhao Q, He T (2015) A novel
753 gene, *optrA*, that confers transferable resistance to oxazolidinones and phenicols and its
754 presence in *Enterococcus faecalis* and *Enterococcus faecium* of human and animal origin. *J*
755 *Antimicrob Chemother* 70: 2182-2190
756 Waterhouse A, Bertoni M, Bienert S, Studer G, Tauriello G, Gumienny R, Heer FT, de Beer
757 TAP, Rempfer C, Bordoli L (2018) SWISS-MODEL: homology modelling of protein structures
758 and complexes. *Nucleic Acids Res* 46: W296-W303
759 Weaver KE, Chen Y, Miiller EM, Johnson JN, Dangler AA, Manias DA, Clem AM, Schjodt DJ,
760 Dunny GM (2017) Examination of *Enterococcus faecalis* toxin-antitoxin system toxin Fst
761 function utilizing a pheromone-inducible expression vector with tight repression and broad
762 dynamic range. *J Bacteriol* 199: e00065-00017
763 Wilson DN (2014) Ribosome-targeting antibiotics and mechanisms of bacterial resistance.
764 *Nat Rev Microbiol* 12: 35-48
765 Wilson DN, Hauryliuk V, Atkinson GC, O'Neill AJ (2020) Target protection as a key antibiotic
766 resistance mechanism. *Nature Rev Microbiol* 18: 637-648
767 Wilson DN, Schluenzen F, Harms JM, Starosta AL, Connell SR, Fucini P (2008) The
768 oxazolidinone antibiotics perturb the ribosomal peptidyl-transferase center and effect tRNA
769 positioning. *Proc Natl Acad Sci U S A* 105: 13339-13344
770 Zhang C, Zhang P, Wang Y, Liu L, Xu D, Ho Y, Li Y, Fu M, Wang X, Wang S (2020)
771 Capsular serotypes, antimicrobial susceptibility, and the presence of transferable
772 oxazolidinone resistance genes in *Streptococcus suis* isolated from healthy pigs in China.
773 *Vet Microbiol* 247: 108750
774 Zhang K (2016) Gctf: Real-time CTF determination and correction. *J Struct Biol* 193: 1-12
775 Zheng SQ, Palovcak E, Armache J-P, Verba KA, Cheng Y, Agard DA (2017) MotionCor2:
776 anisotropic correction of beam-induced motion for improved cryo-electron microscopy. *Nat*
777 *Methods* 14: 331-332
778 Zivanov J, Nakane T, Forsberg BO, Kimanius D, Hagen WJ, Lindahl E, Scheres SH (2018)
779 New tools for automated high-resolution cryo-EM structure determination in RELION-3. *Elife*
780 7: e42166
781 Allignet J, Loncle V, El Solh N (1992) Sequence of a staphylococcal plasmid gene, *vga*,
782 encoding a putative ATP-binding protein involved in resistance to virginiamycin A-like
783 antibiotics. *Gene* 117: 45-51

784 Andersen CBF, Becker T, Blau M, Anand M, Halic M, Balar B, Mielke T, Boesen T, Pedersen
785 JS, Spahn CMT *et al* (2006) Structure of eEF3 and the mechanism of transfer RNA release
786 from the E-site. *Nature* 443: 663-668
787 Antonelli A, D'Andrea MM, Brenciani A, Galeotti CL, Morroni G, Pollini S, Varaldo PE,
788 Rossolini GM (2018) Characterization of poxtA, a novel phenicol–oxazolidinone–tetracycline
789 resistance gene from an MRSA of clinical origin. *J Antimicrob Chemother* 73: 1763-1769
790 Arenz S, Nguyen F, Beckmann R, Wilson DN (2015) Cryo-EM structure of the tetracycline
791 resistance protein TetM in complex with a translating ribosome at 3.9-Å resolution. *Proc Natl*
792 *Acad Sci U S A* 112: 5401-5406
793 Arnaud M, Chastanet A, Débarbouillé M (2004) New vector for efficient allelic replacement in
794 naturally nontransformable, low-GC-content, gram-positive bacteria. *Appl Environ Microbiol*
795 70: 6887-6891
796 Becker T, Franckenberg S, Wickles S, Shoemaker CJ, Anger AM, Armache J-P, Sieber H,
797 Ungewickell C, Berninghausen O, Daberkow I (2012) Structural basis of highly conserved
798 ribosome recycling in eukaryotes and archaea. *Nature* 482: 501-506
799 Bhardwaj P, Ziegler E, Palmer KL (2016) Chlorhexidine induces VanA-type vancomycin
800 resistance genes in enterococci. *Antimicrobial agents and chemotherapy* 60: 2209-2221
801 Camargo AC, Woodward JJ, Nero LA (2016) The continuous challenge of characterizing the
802 foodborne pathogen *Listeria monocytogenes*. *Foodborne Pathog Dis* 13: 405-416
803 Candiano G, Bruschi M, Musante L, Santucci L, Ghiggeri GM, Carnemolla B, Orecchia P,
804 Zardi L, Righetti PG (2004) Blue silver: a very sensitive colloidal Coomassie G-250 staining
805 for proteome analysis. *Electrophoresis* 25: 1327-1333
806 Casañal A, Lohkamp B, Emsley P (2020) Current developments in *Coot* for macromolecular
807 model building of electron cryo-microscopy and crystallographic data. *Protein Sci* 29: 1069-
808 1078
809 Chen B, Boël G, Hashem Y, Ning W, Fei J, Wang C, Gonzalez RL, Hunt JF, Frank J (2014)
810 EttA regulates translation by binding the ribosomal E site and restricting ribosome-tRNA
811 dynamics. *Nat Struct Mol Biol* 21: 152-159
812 Chesneau O, Ligeret H, Hosan-Aghaie N, Morvan A, Dassa E (2005) Molecular analysis of
813 resistance to streptogramin A compounds conferred by the Vga proteins of Staphylococci.
814 *Antimicrob Agents Chemother* 49: 973-980
815 Corrigan RM, Foster TJ (2009) An improved tetracycline-inducible expression vector for
816 *Staphylococcus aureus*. *Plasmid* 61: 126-129
817 Crowe-McAuliffe C, Graf M, Huter P, Takada H, Abdelshahid M, Nováček J, Murina V,
818 Atkinson GC, Hauryliuk V, Wilson DN (2018) Structural basis for antibiotic resistance
819 mediated by the *Bacillus subtilis* ABCF ATPase VmlR. *Proc Natl Acad Sci U S A* 115: 8978-
820 8983

Dar D, Shamir M, Mellin JR, Koutero M, Stern-Ginossar N, Cossart P, Sorek R (2016) Term-seq reveals abundant ribo-regulation of antibiotics resistance in bacteria. *Science* 352: 9822-9822

Davidson AL, Dassa E, Orelle C, Chen J (2008) Structure, function, and evolution of bacterial ATP-binding cassette systems. *Microbiol Mol Biol Rev* 72: 317-364

Davis Dv, McAlpine JB, Pazoles CJ, Talbot MK, Alder EA, White AC, Jonas BM, Murray BE, Weinstock GM, Rogers BL (2001) *Enterococcus faecalis* multi-drug resistance transporters: application for antibiotic discovery. *J Mol Microbiol Biotechnol* 3: 179-184

Dornhelm P, Högenauer G (1978) The effects of tiamulin, a semisynthetic pleuromutilin derivative, on bacterial polypeptide chain initiation. *Eur J Biochem* 91: 465-473

Dorrian J, Kerr I (2009) *Can ABC proteins confer drug resistance in micro-organisms without being export pumps?* Caister Academic Press

Dunkle JA, Xiong L, Mankin AS, Cate JH (2010) Structures of the *Escherichia coli* ribosome with antibiotics bound near the peptidyl transferase center explain spectra of drug action. *Proc Natl Acad Sci U S A* 107: 17152-17157

Duval M, Dar D, Carvalho F, Rocha EP, Sorek R, Cossart P (2018) HflXr, a homolog of a ribosome-splitting factor, mediates antibiotic resistance. *Proc Natl Acad Sci U S A* 115: 13359-13364

Ero R, Kumar V, Su W, Gao YG (2019) Ribosome protection by ABC-F proteins—Molecular mechanism and potential drug design. *Protein Sci* 28: 684-693

Fairweather N, Kennedy S, Foster T, Kehoe M, Dougan G (1983) Expression of a cloned *Staphylococcus aureus* α-hemolysin determinant in *Bacillus subtilis* and *Staphylococcus aureus*. *Infect Immun* 41: 1112-1117

Fischer N, Neumann P, Konevega AL, Bock LV, Ficner R, Rodnina MV, Stark H (2015) Structure of the *E. coli* ribosome–EF-Tu complex at < 3 Å resolution by Cs-corrected cryo-EM. *Nature* 520: 567-570

Fostier CR, Monlezun L, Ousalem F, Singh S, Hunt JF, Boël G (2020) ABC-F translation factors: from antibiotic resistance to immune response. *FEBS Lett*

Freitas AR, Elghaieb H, León-Sampedro R, Abbassi MS, Novais C, Coque TM, Hassen A, Peixe L (2017) Detection of *optrA* in the African continent (Tunisia) within a mosaic *Enterococcus faecalis* plasmid from urban wastewaters. *J Antimicrob Chemother* 72: 3245-3251

Gabdulkhakov A, Tishchenko S, Mikhaylina A, Garber M, Nevskaya N, Nikonov S (2017) Crystal Structure of the 23S rRNA Fragment Specific to r-Protein L1 and Designed Model of the Ribosomal L1 Stalk from Haloarcula marismortui. *Crystals* 7: 37

Gerovac M, Tampé R (2019) Control of mRNA translation by versatile ATP-driven machines. *Trends Biochem Sci* 44: 167-180

Glaser P, Frangeul L, Buchrieser C, Rusniok C, Amend A, Baquero F, Berche P, Bloecker H, Brandt P, Chakraborty T (2001) Comparative genomics of *Listeria* species. *Science* 294: 849-852

Golubev A, Fatkhullin B, Khusainov I, Jenner L, Gabdulkhakov A, Validov S, Yusupova G, Yusupov M, Usachev K (2020) Cryo-EM structure of the ribosome functional complex of the human pathogen *Staphylococcus aureus* at 3.2 Å resolution. *FEBS letters*

Henderson R, Sali A, Baker ML, Carragher B, Devkota B, Downing KH, Egelman EH, Feng Z, Frank J, Grigorieff N (2012) Outcome of the first electron microscopy validation task force meeting. *Structure* 20: 205-214

Heuer A, Gerovac M, Schmidt C, Trowitzsch S, Preis A, Kötter P, Berninghausen O, Becker T, Beckmann R, Tampe R (2017) Structure of the 40S–ABCE1 post-splitting complex in ribosome recycling and translation initiation. *Nat Struct Mol Biol* 24: 453-460

Ho SN, Hunt HD, Horton RM, Pullen JK, Pease LR (1989) Site-directed mutagenesis by overlap extension using the polymerase chain reaction. *Gene* 77: 51-59

Horsburgh MJ, Aish JL, White IJ, Shaw L, Lithgow JK, Foster SJ (2002) σB modulates virulence determinant expression and stress resistance: characterization of a functional rsbU strain derived from *Staphylococcus aureus* 8325-4. *J Bacteriol* 184: 5457-5467

Hot C, Berthet N, Chesneau O (2014) Characterization of *sal*(A), a novel gene responsible for lincosamide and ttreptogramin A resistance in *Staphylococcus sciuri*. *Antimicrob Agents Chemother* 58: 3335-3341

Iimura M, Hayashi W, Arai E, Natori T, Horiuchi K, Matsumoto G, Tanaka H, Soga E, Nagano Y, Arakawa Y (2020) Identification of a multiresistant mosaic plasmid carrying a new segment of *IS1216E*-flanked *optrA* with integrated Tn551-*ermB* element in linezolid-resistant *Enterococcus faecalis* human isolate. *J Glob Antimicrob Res* 22: 679-699

Jacquet E, Girard JM, Ramaen O, Pamlard O, Lévaique H, Betton JM, Dassa E, Chesneau O (2008) ATP hydrolysis and pristinamycin IIA inhibition of the *Staphylococcus aureus* Vga(A), a dual ABC protein involved in streptogramin A resistance. *J Biol Chem* 283: 25332-25339

James NR, Brown A, Gordiyenko Y, Ramakrishnan V (2016) Translational termination without a stop codon. *Science* 354: 1437-1440

Johnson ZL, Chen J (2018) ATP binding enables substrate release from Multidrug Resistance Protein 1. *Cell* 172: 81-89

Khusainov I, Vicens Q, Bochler A, Grosse F, Myasnikov A, Ménétret J-F, Chicher J, Marzi S, Romby P, Yusupova G (2016) Structure of the 70S ribosome from human pathogen *Staphylococcus aureus*. *Nucleic Acids Res* 44: 10491-10504

Kirchner S, Rauscher R, Czech A, Ignatova Z (2017) Microarray-based quantification of cellular tRNAs. *Protocolsio*

895 Koberska M, Vesela L, Vimberg V, Lenart J, Vesela J, Kamenik Z, Janata J, Novotna GB
896 (2020) Beyond self-resistance: ABCF ATPase LmrC is a signal-transducing component of an
897 antibiotic-driven signaling cascade hastening the onset of lincomycin biosynthesis. *bioRxiv*:
898 2020.2010.2016.343517
899 Krishnan A, Burroughs AM, Iyer LM, Aravind L (2020) Comprehensive classification of ABC
900 ATPases and their functional radiation in nucleoprotein dynamics and biological conflict
901 systems. *Nucleic Acids Res* 48: 10045–10075
902 Kucukelbir A, Sigworth FJ, Tagare HD (2014) Quantifying the local resolution of cryo-EM
903 density maps. *Nat Methods* 11: 63-65
904 Lenart J, Vimberg V, Vesela L, Janata J, Novotna GB (2015) Detailed mutational analysis of
905 Vga(A) interdomain linker: Implication for antibiotic resistance specificity and mechanism.
906 *Antimicrob Agents Chemother* 59: 1360-1364
907 Liebschner D, Afonine PV, Baker ML, Bunkóczi G, Chen VB, Croll TI, Hintze B, Hung L-W,
908 Jain S, McCoy AJ (2019) Macromolecular structure determination using X-rays, neutrons and
909 electrons: recent developments in Phenix. *Acta Crystallogr D Struct Biol* 75: 861-877
910 Loveland AB, Demo G, Grigorieff N, Korostelev AA (2017) Ensemble cryo-EM elucidates the
911 mechanism of translation fidelity. *Nature* 546: 113-117
912 Magill SS, Edwards JR, Bamberg W, Beldavs ZG, Dumyati G, Kainer MA, Lynfield R,
913 Maloney M, McAllister-Hollod L, Nadle J (2014) Multistate point-prevalence survey of health
914 care-associated infections. *N Engl J Med* 370: 1198-1208
915 Mamtora D, Saseedharan S, Bhalekar P, Katakdhond S (2019) Microbiological profile and
916 antibiotic susceptibility pattern of Gram-positive isolates at a tertiary care hospital. *J Lab*
917 *Physicians* 11: 144-148
918 Marks J, Kannan K, Roncase EJ, Klepacki D, Kefi A, Orelle C, Vazquez-Laslop N, Mankin
919 AS (2016) Context-specific inhibition of translation by ribosomal antibiotics targeting the
920 peptidyl transferase center. *Proc Natl Acad Sci U S A* 113: 12150-12155
921 Matzov D, Eyal Z, Benhamou RI, Shalev-Benami M, Halfon Y, Krupkin M, Zimmerman E,
922 Rozenberg H, Bashan A, Fridman M (2017) Structural insights of lincosamides targeting the
923 ribosome of *Staphylococcus aureus*. *Nucleic Acids Res* 45: 10284-10292
924 Mendes RE, Paukner S, Doyle TB, Gelone SP, Flamm RK, Sader HS (2019) Low
925 Prevalence of Gram-positive isolates showing elevated lefamulin MIC results during the
926 SENTRY Surveillance Program for 2015–2016 and characterization of resistance
927 mechanisms. *Antimicrob Agents Chemother* 63: e02158-02118
928 Meydan S, Marks J, Klepacki D, Sharma V, Baranov PV, Firth AE, Margus T, Kefi A,
929 Vázquez-Laslop N, Mankin AS (2019) Retapamulin-assisted ribosome profiling reveals the
930 alternative bacterial proteome. *Mol Cell* 74: 481-493

931 Monk IR, Gahan CG, Hill C (2008) Tools for functional postgenomic analysis of *Listeria*
932 *monocytogenes*. *Appl Environ Microbiol* 74: 3921-3934
933 Moriya T, Saur M, Stabrin M, Merino F, Voicu H, Huang Z, Penczek PA, Raunser S,
934 Gatsogiannis C (2017) High-resolution single particle analysis from electron cryo-microscopy
935 images using SPHIRE. *J Vis Exp*: e55448
936 Murina V, Kasari M, Hauryliuk V, Atkinson GC (2018) Antibiotic resistance ABCF proteins
937 reset the peptidyl transferase centre of the ribosome to counter translational arrest. *Nucleic*
938 *Acids Res*: 1-11
939 Murina V, Kasari M, Takada H, Hinnu M, Saha CK, Grimshaw JW, Seki T, Reith M, Putrinš
940 M, Tenson T (2019) ABCF ATPases involved in protein synthesis, ribosome assembly and
941 antibiotic resistance: structural and functional diversification across the tree of life. *J Mol Biol*
942 431: 3568-3590
943 Murphy EL, Singh KV, Avila B, Kleffmann T, Gregory ST, Murray BE, Krause KL, Khayat R,
944 Jogl G (2020) Cryo-electron microscopy structure of the 70S ribosome from *Enterococcus*
945 *faecalis*. *Sci Rep* 10: 16301
946 Noeske J, Wasserman MR, Terry DS, Altman RB, Blanchard SC, Cate JH (2015) High-
947 resolution structure of the *Escherichia coli* ribosome. *Nat Struct Mol Biol* 22: 336-341
948 Novotna G, Janata J (2006) A new evolutionary variant of the streptogramin A resistance
949 protein, Vga(A)$_{LC}$, from *Staphylococcus haemolyticus* with shifted substrate specificity
950 towards lincosamides. *Antimicrob Agent Chemother* 50: 4070-4076
951 Ohki R, Tateno K, Takizawa T, Aiso T, Murata M (2005) Transcriptional termination control of
952 a novel ABC transporter gene involved in antibiotic resistance in *Bacillus subtilis*. *J Bacteriol*
953 187: 5946-5954
954 Orelle C, Carlson S, Kaushal B, Almutairi MM, Liu H, Ochabowicz A, Quan S, Pham VC,
955 Squires CL, Murphy BT (2013) Tools for characterizing bacterial protein synthesis inhibitors.
956 *Antimicrob Agent Chemother* 57: 5994-6004
957 Ousalem F, Singh S, Chesneau O, Hunt JF, Boël G (2019) ABC-F proteins in mRNA
958 translation and antibiotic resistance. *Res Microbiol* 170: 435-447
959 O'Neill A (2010) *Staphylococcus aureus* SH1000 and 8325-4: comparative genome
960 sequences of key laboratory strains in staphylococcal research. *Letters in applied*
961 *microbiology* 51: 358-361
962 Pettersen EF, Goddard TD, Huang CC, Couch GS, Greenblatt DM, Meng EC, Ferrin TE
963 (2004) UCSF Chimera—a visualization system for exploratory research and analysis. *J*
964 *Comp Chem* 25: 1605-1612
965 Pfaller MA, Cormican M, Flamm RK, Mendes RE, Jones RN, 2019. Temporal and
966 geographic variation in antimicrobial susceptibility and resistance patterns of enterococci:

967 results from the SENTRY Antimicrobial Surveillance Program, 1997-2016, Open Forum
968 Infect Dis. Oxford University Press US, pp. S54-S62.
969 Polacek N, Mankin AS (2005) The ribosomal peptidyl transferase center: structure, function,
970 evolution, inhibition. *Crit Rev Biochem Mol Biol* 40: 285-311
971 Polikanov YS, Starosta AL, Juette MF, Altman RB, Terry DS, Lu W, Burnett BJ, Dinos G,
972 Reynolds KA, Blanchard SC *et al* (2015) Distinct tRNA accommodation intermediates
973 observed on the ribosome with the antibiotics Hygromycin A and A201A. *Mol Cell* 58: 832-
974 844
975 Polikanov YS, Steitz TA, Innis CA (2014) A proton wire to couple aminoacyl-tRNA
976 accommodation and peptide-bond formation on the ribosome. *Nat Struct Mol Biol* 21: 787-
977 793
978 Pulk A, Cate JH (2013) Control of ribosomal subunit rotation by elongation factor G. *Science*
979 340: 1-7
980 Ranjan N, Pochopien AA, Wu CC-C, Beckert B, Blanchet S, Green R, Rodnina MV, Wilson
981 DN (2020) eEF3 promotes late stages of tRNA translocation on the ribosome. *bioRxiv*
982 Rees DC, Johnson E, Lewinson O (2009) ABC transporters: the power to change. *Nat Rev*
983 *Mol Cell Biol* 10: 218-227
984 Reynolds ED, Cove JH (2005) Resistance to telithromycin is conferred by *msr*(A), *msrC* and
985 *msr*(D) in *Staphylococcus aureus*. *J Antimicrob Chemother* 56: 1179-1180
986 Rohou A, Grigorieff N (2015) CTFFIND4: Fast and accurate defocus estimation from electron
987 micrographs. *J Struct Biol* 192: 216-221
988 Ross JI, Eady EA, Cove JH, Cunliffe WJ, Baumberg S, Wootton JC (1990) Inducible
989 erythromycin resistance in staphlyococci is encoded by a member of the ATP-binding
990 transport super-gene family. *Mol Microbiol* 4: 1207-1214
991 Ross JI, Farrell AM, Eady EA, Cove JH, Cunliffe WJ (1989) Characterisation and molecular
992 cloning of the novel macrolide-streptogramin B resistance determinant from *Staphylococcus*
993 *epidermidis*. *J Antimicrob Chemother* 24: 851-862
994 Rozov A, Khusainov I, El Omari K, Duman R, Mykhaylyk V, Yusupov M, Westhof E, Wagner
995 A, Yusupova G (2019) Importance of potassium ions for ribosome structure and function
996 revealed by long-wavelength X-ray diffraction. *Nat Commun* 10: 1-12
997 Sadowy E (2018) Linezolid resistance genes and genetic elements enhancing their
998 dissemination in enterococci and streptococci. *Plasmid* 99: 89-98
999 Schenk S, Laddaga RA (1992) Improved method for electroporation of *Staphylococcus*
1000 *aureus*. *FEMS Microbiol Lett* 94: 133-138
1001 Scheres SH, Chen S (2012) Prevention of overfitting in cryo-EM structure determination. *Nat*
1002 *Methods* 9: 853-854

1003 Schlünzen F, Pyetan E, Fucini P, Yonath A, Harms JM (2004) Inhibition of peptide bond
1004 formation by pleuromutilins: the structure of the 50S ribosomal subunit from *Deinococcus*
1005 *radiodurans* in complex with tiamulin. *Mol Microbiol* 54: 1287-1294
1006 Sharkey LK, Edwards TA, O'Neill AJ (2016) ABC-F proteins pediate antibiotic resistance
1007 through ribosomal protection. *mBio* 7: e01975
1008 Sharkey LK, O'Neill AJ (2018) Antibiotic resistance ABC-F proteins: bringing target protection
1009 into the limelight. *ACS Infect Dis* 4: 239-246
1010 Simon R, Priefer U, Pühler A (1983) A broad host range mobilization system for *in vivo*
1011 genetic engineering: transposon mutagenesis in Gram negative bacteria. *Bio/technology* 1:
1012 784-791
1013 Singh KV, Malathum K, Murray BE (2001) Disruption of an *Enterococcus faecium* species-
1014 specific gene, a homologue of acquired macrolide resistance genes of staphylococci, is
1015 associated with an increase in macrolide susceptibility. *Antimicrob Agent Chemother* 45:
1016 263-266
1017 Singh KV, Weinstock GM, Murray BE (2002) An *Enterococcus faecalis* ABC homologue
1018 (Lsa) is required for the resistance of this species to clindamycin and quinupristin-dalfopristin.
1019 *Antimicrob Agents Chemother* 46: 1845-1850
1020 Su W, Kumar V, Ding Y, Ero R, Serra A, Lee BST, Wong ASW, Shi J, Sze SK, Yang L
1021 (2018) Ribosome protection by antibiotic resistance ATP-binding cassette protein. *Proc Natl*
1022 *Acad Sci U S A* 115: 5157-5162
1023 Takada H, Roghanian M, Murina V, Dzhygyr I, Murayama R, Akanuma G, Atkinson GC,
1024 Garcia-Pino A, Hauryliuk V (2020) The C-terminal RRM/ACT domain is crucial for fine-tuning
1025 the activation of 'long' RelA-SpoT Homolog enzymes by ribosomal complexes. *Front*
1026 *Microbiol* 11: 277
1027 Thomas C, Tampé R (2020) Structural and mechanistic principles of ABC transporters. *Ann*
1028 *Rev Biochem* 89: 605-636
1029 Tishchenko S, Gabdulkhakov A, Nevskaya N, Sarskikh A, Kostareva O, Nikonova E,
1030 Sycheva A, Moshkovskii S, Garber M, Nikonov S (2012) High-resolution crystal structure of
1031 the isolated ribosomal L1 stalk. *Acta Crystallogr D Biol Crystallogr* 68: 1051-1057
1032 Tu D, Blaha G, Moore PB, Steitz TA (2005) Structures of MLS_BK antibiotics bound to
1033 mutated large ribosomal subunits provide a structural explanation for resistance. *Cell* 121:
1034 257-270
1035 Vimberg V, Cavanagh JP, Novotna M, Lenart J, Nguyen Thi Ngoc B, Vesela J, Pain M,
1036 Koberska M, Balikova Novotna G (2020) Ribosome-mediated attenuation of *vga*(A)
1037 expression is shaped by the antibiotic resistance specificity of Vga(A) protein variants.
1038 *Antimicrob Agent Chemother* 64: e00666-00620

1039 Voorhees RM, Schmeing TM, Kelley AC, Ramakrishnan V (2010) The mechanism for
1040 activation of GTP hydrolysis on the ribosome. *Science* 330: 835-838
1041 Wang Y, Lv Y, Cai J, Schwarz S, Cui L, Hu Z, Zhang R, Li J, Zhao Q, He T (2015) A novel
1042 gene, *optrA*, that confers transferable resistance to oxazolidinones and phenicols and its
1043 presence in *Enterococcus faecalis* and *Enterococcus faecium* of human and animal origin. *J*
1044 *Antimicrob Chemother* 70: 2182-2190
1045 Waterhouse A, Bertoni M, Bienert S, Studer G, Tauriello G, Gumienny R, Heer FT, de Beer
1046 TAP, Rempfer C, Bordoli L (2018) SWISS-MODEL: homology modelling of protein structures
1047 and complexes. *Nucleic Acids Res* 46: W296-W303
1048 Weaver KE, Chen Y, Miiller EM, Johnson JN, Dangler AA, Manias DA, Clem AM, Schjodt DJ,
1049 Dunny GM (2017) Examination of *Enterococcus faecalis* toxin-antitoxin system toxin Fst
1050 function utilizing a pheromone-inducible expression vector with tight repression and broad
1051 dynamic range. *J Bacteriol* 199: e00065-00017
1052 Wilson DN (2014) Ribosome-targeting antibiotics and mechanisms of bacterial resistance.
1053 *Nat Rev Microbiol* 12: 35-48
1054 Wilson DN, Hauryliuk V, Atkinson GC, O'Neill AJ (2020) Target protection as a key antibiotic
1055 resistance mechanism. *Nature Rev Microbiol* 18: 637-648
1056 Wilson DN, Schluenzen F, Harms JM, Starosta AL, Connell SR, Fucini P (2008) The
1057 oxazolidinone antibiotics perturb the ribosomal peptidyl-transferase center and effect tRNA
1058 positioning. *Proc Natl Acad Sci U S A* 105: 13339-13344
1059 Zhang C, Zhang P, Wang Y, Liu L, Xu D, Ho Y, Li Y, Fu M, Wang X, Wang S (2020)
1060 Capsular serotypes, antimicrobial susceptibility, and the presence of transferable
1061 oxazolidinone resistance genes in *Streptococcus suis* isolated from healthy pigs in China.
1062 *Vet Microbiol* 247: 108750
1063 Zhang K (2016) Gctf: Real-time CTF determination and correction. *J Struct Biol* 193: 1-12
1064 Zheng SQ, Palovcak E, Armache J-P, Verba KA, Cheng Y, Agard DA (2017) MotionCor2:
1065 anisotropic correction of beam-induced motion for improved cryo-electron microscopy. *Nat*
1066 *Methods* 14: 331-332
1067 Zivanov J, Nakane T, Forsberg BO, Kimanius D, Hagen WJ, Lindahl E, Scheres SH (2018)
1068 New tools for automated high-resolution cryo-EM structure determination in RELION-3. *Elife*
1069 7: e42166
1070
1071

Materials and methods

Strains and plasmids

All strains and plasmids used in this work are listed in Table S5.

E. faecalis OG1RF and TX5332, a LsaA disruption mutant of OG1RF (Singh *et al.*, 2002), were kindly provided by Dr. Barbara E. Murray (Health Science Center, University of Texas). All cloning was performed by Protein Expertise Platform at Umeå University. *E. faecalis* LsaA ORF was PCR amplified from pTEX5333 plasmid and cloned into either $pCIE_{cam}$ (Weaver *et al.*, 2017) (used for preparation of LsaA-70S complexes) or $pCIE_{cam}$ ($pCIE_{cam}$ derivative with the Cm^r gene swapped to the spectinomycin resistance Sc^r gene; used for MIC testing) vector for cCF10-inducible expression. To allow detection by immunoblotting and preparation of LsaA-70S complexes, the LsaA ORF was supplemented with C-terminal His_6-TEV-$FLAG_3$-tag (HTF tag) and the ribosome binding site was optimized for high expression yield. Point mutations $E_{142}Q$ and $E_{452}Q$ were introduced to LsaA resulting in pCIE_LsaA-EQ_2-HTF.

S. haemolyticus *vga(A)$_{LC}$* gene was PCR-amplified from a *S. haemolyticus* isolate held in the O'Neill strain collection at the University of Leeds, using oligonucleotide primers vgaALC-F (5′-GGTGGTGGTACCAGGATGAGGAAATATGAAAA-3′) and $vgaA_{LC}$-R (5′-GGTGGTGAATTCGGTAATTTATTTATCTAAATTTCTT-3′) (engineered restriction sites shown underlined). The protein encoded by this gene is identical to that previously reported (Novotna & Janata, 2006) (accession number DQ823382). The fragment was digested with *Kpn*I and *Eco*RI and ligated into the tetracycline-inducible expression vector pRMC2 (Corrigan & Foster, 2009). Constructs encoding the $VgaA_{LC}$ protein fused with a C-terminal $FLAG_3$ tag were obtained by synthesis (Genewiz), with $E_{105}Q$, $E_{410}Q$ and EQ_2 mutants subsequently created by site-directed mutagenesis. Generation of other point mutants of untagged $Vga(A)_{LC}$ was performed by NBS Biologicals, again using chemical synthesis to generate the original *vga(A)$_{LC}$* template, followed by site-directed mutagenesis.

L. monocytogenes VgaL (Lmo0919). In order to construct *L. monocytogenes* EDGe::Δ*lmo0919*, regions corresponding to the upstream and downstream flanking regions of *lmo0919*, present on the EDGe genome were amplified with primer pairs VKT35 (5′-GGGGGGATCCATCACTAGCCGAATCCAAAC-3′), VKT36 (5′-GGGGGAATTCAAAAAATAACCTCCTGAATATTTTCAGAG-3′) and VHKT37 (5′-GGGGGAATTCATTGTTGTCTTTTTATTCAAGCTAAATAAAAAA-3′), VHKT38 (5′-GGGGCCATGGCGTGCTGTACGGTATGC-3′) respectively. Fragments were then cloned in tandem into the pMAD vector using *Bam*HI, *Eco*RI and *Nco*RI restriction sites. The resulting vector, VHp689, was then sequenced to ensure wild-type sequences of clones. Gene deletion was then performed as per Arnaud *et. al.* (Arnaud *et al*, 2004).

lmo0919 was amplified from EDGe genomic DNA using primers VHKT12 (5′-CCCCCCATGGCATCTACAATCGAAATAAATC-3′) and VHKT39 (5′-GGGGCTGCAGTTAACTAAATTGCTGTCTTTTTG-3′), and cloned into pIMK3 using *Nco*I and *Pst*I restriction sites, resulting in plasmid VHp690.

Overlap extension PCR was used in order to introduce a HTF tag at the C-terminus of *lmo0919* (Ho *et al*, 1989). The *lmo0919* locus and HTF tag were amplified with primer pairs VHKT12, VHKT15 (5′-ATGATGATGGCCGCCACTAAATTGCTGTCTTTTTG-3′) and VHKT14 (5′-AGACAGCAATTTAGTGGCGGCCATCATCATCATC-3′), VHKT13 (5′-GGGGCTGCAGTTAGCCTTTGTCATCGTC-3′) using EDGe genomic DNA and VHp100 template DNA respectively, producing fragments with overlapping ends. VHKT12 and VHKT13 were then used to fuse the fragments and the resulting PCR product was cloned into pIMK3 using *Nco*I and *Pst*I sites resulting in VHp692.

To introduce EQ2 mutations (E104Q and E408Q) simultaneously into the VHp692 plasmid, primers VHT266 (5′-TCTTGATCAACCAACCAACTATTTGGATATCTACGCAATGGAA-3′) and VHT267 (5′-TTGTTGGTTGGTCTGCTAGGAGAACACTTGGATTTTGGCGCA-3′) containing both mutations were used to extend out from *lmo0919*^{HTF} to amplify the VHp692 backbone. Primers VHT264 (5′-AGCAGACCAACCAACAAGCAATCTTGATGTCG-3′) and VHT265 (5′-TGGTTGGTTGATCAAGAATCAAGAAATTGGCGT-3′) also containing *lmo0919*^{EQ2} mutations were used to amplify a fragment with overlapping sequence to the backbone fragment. Both PCR products were then assembled using NEBuilder® HiFi DNA Assembly Master Mix (NEB), resulting in VHp693.

B. subtilis: To construct the VHB109 [*trpC2* Δ*vmlR* thrC::P$_{hy\text{-}spnak}$-*lsaA kmR*] strain untagged LsaA under the control of an IPTG-inducible P$_{hy\text{-}spank}$ promotor, a PCR product encoding lsa(A) was PCR-amplified from pTEX5333 using the primers VHT127 (5′-CGACGAAGGAGAGAGCGATAATGTCGAAAATTGAACTAAAACAACTATC-3′) and VHT128 (5′-CACCGAATTAGCTTGCATGCTTATGATTTCAAGACAATTTTTTTATCTGTTA-3′). The second PCR fragment encoding a kanamycin-resistance marker, a polylinker downstream of the Phy-spank promoter and the lac repressor ORF – all inserted in the middle of the thrC gene – was PCR-amplified from pHT009 plasmid using primers VHT123 (5′-CATTATCGCTCTCTCCTTCGTCGACTAAGCTAATTG-3′) and VHT125 (5′-TAAGCATGCAAGCTAATTCGGTGGAAACGAGG-3′). The two fragments were ligated using the NEBuilder HiFi DNA Assembly master mix (New England BioLabs, Ipswich, MA) yielding the pHT009-lsaA plasmid (VHp369) which was used to transform the VHB5 [*trpC2* Δ*vmlR*] strain. Selection for kanamycin resistance yielded the desired VHB109 strain. To construct the VHB168 [*trpC2* Δ*vmlR* thrC::P$_{hy\text{-}spnak}$-*lsaAK244A kmR*] strain, VHp369 plasmid was subjected to site-directed mutagenesis using primer VHP303 (5′-GCATCACCTTCACGGTTCATCGACCATTCCGCT-3′) and VHP304 (5′-

GTACGGCAACGCTAAGGAAAAAGGGAGCGGGGCGA-3′), according to directions of Phusion Site-Directed Mutagenesis Kit (Thermo Fisher Scientific), yielding, yielding VHp526 (pHT009-*lsaAK244A*) plasmid which was used to transform the VHB5 [*trpC2* Δ*vmlR*] strain. Selection for kanamycin resistance yielded the desired VHB168 strain. To construct the VHB169 [*trpC2* Δ*vmlR thrC*::$P_{hy\text{-}spnak}$-*lsaAF257A kmR*] strain, VHp369 plasmid was subjected to site-directed mutagenesis using primer VHP305 (5′-CAATCGCCCCGCTCCCTTTTTCCTTAGCGT-3′) and VHP306 (5′-CGGATACAGGAGCCATTGGTGCCCGGGCA-3′) , according to directions of Phusion Site-Directed Mutagenesis Kit (Thermo Fisher Scientific), yielding, yielding VHp527 (pHT009-*lsaAF257A*) plasmid which was used to transform the VHB5 [*trpC2* Δ*vmlR*] strain. Selection for kanamycin resistance yielded the desired VHB169 strain.

Bacterial transformation

E. faecalis: Electrocompetent cells were prepared as per Bhardwaj and colleagues (Bhardwaj *et al*, 2016). Shortly, an over-night culture grown in the presence of appropriate antibiotics was diluted to OD_{600} of 0.05 in 50 mL of BHI media (supplemented with 2 mg/mL kanamycin in case of TX5332), grown to OD_{600} of 0.6-0.7 at 37 °C with moderate shaking (160 rpm). Cells were collected by centrifugation at 4,000 rpm at 4 °C for 10 min. Cells were resuspended in 0.5 mL of sterile lysozyme buffer (10 mM Tris-HCl pH 8; 50 mM NaCl, 10 mM EDTA, 35 µg/mL lysozyme), transferred to 1.5 mL Eppendorf tube and incubated at 37 °C for 30 minutes. Cells were pelleted at 10,000 rpm at 4 °C for 10 min and washed three times with 1.5 mL of ice-cold electroporation buffer (0.5M sucrose, 10% glycerol(w/v)). After last wash the cells were resuspended in 500 µL of ice-cold electroporation buffer and aliquoted and stored at –80°C. For electroporation 35 µL of electrocompetent cells were supplemented with 1 µg of plasmid DNA, transferred to ice-cold 1 mm electroporation cuvette and electroporated at 1.8 keV. Immediately after electroporation 1 mL of ice-cold BHI was added to the cells, the content of the cuvette was transferred to 1.5 mL Eppendorf tubes and the cells were recovered at 37 °C for 2.5 hours and plated to BHI plates containing appropriate antibiotics (10 µg/mL chloramphenicol and 2 mg/mL kanamycin).

S. aureus: the preparation and transformation of *S. aureus* electrocompetent cells followed the method of Schenk & Laddaga (Schenk & Laddaga, 1992), though used Tryptone soya broth (Oxoid) containing 2.5% yeast extract in place of B2 medium. Sequence-verified constructs established in *E. coli* were transferred into the restriction deficient *S. aureus* RN4220 strain (Fairweather *et al*, 1983), before recovery and introduction into *S. aureus* SH1000 (Horsburgh *et al*, 2002; O'Neill, 2010).

L. monocytogenes: pIMK3 integrative plasmids were transformed into *L. monocytogenes* via conjugation. *E. coli* S17.1 harbouring pIMK3 and its derivatives, was grown at 37 °C overnight in LB media supplemented with 50 µg/mL Kanamycin, 1 mL of culture was washed three times with sterile BHI media to remove antibiotics. 200 µL of washed *E. coli* culture was mixed with an equal volume of *L. monocytogenes* overnight culture grown at 37 °C in BHI media. 200 µl of mixed bacterial suspension was then dropped onto a conjugation filter (Millipore #HAEP047S0) placed onto a BHI agar plate containing 0.2 µg/mL penicillin-G. After overnight incubation at 37 °C, bacterial growth from the filter was re-suspended in 1 ml of BHI and 100-300 µL plated onto BHI-agar plates supplemented with 50 µg/mL Kanamycin (to select for pIMK3), 50 µg/mL Nalidixic acid and 10 µg/mL Colistin sulfate (Sigma-Aldrich C4461-100MG). Resulting colonies were checked for correct integration via PCR and subsequent sequencing using primers VHKT42 and VHKT43.

Antibiotic susceptibility testing

Minimum Inhibitory Concentrations (MIC) were determined based on guidelines from the European Committee on Antimicrobial Susceptibility Testing (EUCAST) (http://www.eucast.org/ast_of_bacteria/mic_determination).

E. faecalis: bacteria were grown in BHI media supplemented with 2 mg/mL kanamycin (to prevent *lsa* revertants), either 0.1 mg/mL spectinomycin (to maintain the $pCIE_{spec}$ plasmid),) or 20 µg/mL of chloramphenicol (to maintain the $pCIE_{cam}$ plasmid used to validate the functionality of the HTF-tagged LsaA variant), 100 ng/mL of cCF10 peptide (to induce expression of LsaA protein) as well as increasing concentrations of antibiotics was inoculated with 5×10^5 CFU/mL (OD_{600} of approximately 0.0005) of *E. faecalis* Δ*lsaA* (*lsa::Kan*) strain TX5332 transformed either with empty $pCIE_{spec}$ plasmid, or with $pCIE_{spec}$ encoding LsaA. After 16-20 hours at 37 °C without shaking, the presence or absence of bacterial growth was scored by eye.

S. aureus: bacteria were grown in cation-adjusted Mueller-Hinton Broth (MHB) at 37 °C with vigorous aeration, supplemented with 10 mg/L chloramphenicol to maintain the pRMC2 plasmid. Upon reaching an absorbance of OD_{625} of 0.6, anhydrotetracycline (ATC) (Sigma-Aldrich, UK) was added at a final concentration of 100 ng/mL to induce expression from pRMC2, and incubated for a further 3 hours. Cultures were then diluted to 5×10^5 CFU/mL using MHB supplemented with ATC (100 ng/mL) and used in MIC determinations essentially as described above (though cultures were shaken).

L. monocytogenes: bacteria were grown in BHI media supplemented with 50 µg/mL kanamycin (to prevent loss of the integrated pIMK3 plasmid), 1 mM of IPTG (to induce expression of VgaL protein) as well as increasing concentrations of antibiotics was inoculated

with 5 x 10^5 CFU/mL (OD_{600} of approximately 0.0003) of *L. monocytogenes* EDG-*e* wildtype strain or EDG-*e*::Δ*lmo0919* strain transformed either with empty pIMK3 plasmid, or with pIMK3 encoding VgaL variants. After 16–20 hours at 37 °C without shaking, the presence or absence of bacterial growth was scored by eye.

B. subtilis (for LsaA mutants): *B. subtilis* strains were pre-grown on LB plates either supplemented with 1 mM IPTG overnight at 30 °C. Fresh individual colonies were used to inoculate filtered LB medium in the presence of 1 mM IPTG, and OD_{600} adjusted to 0.01. The cultures were seeded on a 100-well honeycomb plate (Oy Growth Curves AB Ltd, Helsinki, Finland), and plates incubated in a Bioscreen C (Labsystems, Helsinki, Finland) at 37°C with continuous medium shaking. After 90 min ($OD_{600} \approx 0.1$), antibiotics were added and growth was followed for an additional 6 hours.

Preparation of bacterial lysates

Preparation of bacterial biomass

E. faecalis: *E. faecalis* TX5332 transformed with pCIE plasmids (either empty vector and expressing either wild-type or EQ_2 variants of C-terminally HTF-tagged LsaA) were grown overnight from single colony in BHI supplemented with 2 mg/mL kanamycin and 10 µg/mL of chloramphenicol. Next day overnight cultures were diluted to starting OD_{600} of 0.05 in 160 mL BHI supplemented with 0.5 mg/mL kanamycin and 10 µg/mL of chloramphenicol. Cells were grown with intensive shaking at 37 °C till OD_{600} of 0.6 and were induced with 300 ng/mL of cCF10 peptide for 30 minutes prior harvesting by centrifugation at 10,000 ×g for 15 minutes at 4 °C.

S. aureus: *S. aureus* SH1000 transformed with pRMC2 plasmids (empty vector, wild-type and EQ_2 $VgaA_{LC}$-$FLAG_3$) were grown in LB supplemented with 25 µg/mL of chloramphenicol. Saturated cultures were diluted to an OD_{600} of 0.1 in 400 mL LB supplemented with 20 µg/mL of chloramphenicol and grown at 37 °C with vigorous aeration to an OD_{600} of 0.6. Protein expression was induced with 100 ng/mL of anhydro-tetracycline for 30 minutes prior to harvesting by centrifugation at 10 000 ×g for 15 minutes at 4 °C.

L. monocytogenes: *L. monocytogenes* EDG-*e* was transformed with pIMK3 plasmids (empty vector, wild-type and EQ_2 VgaL-HTF) were grown overnight from single colony in LB supplemented with 50 µg/mL of kanamycin. Next day overnight cultures were diluted till starting OD_{600} of 0.005 in 200 mL BHI supplemented with 50 µg/mL of Kanamycin. Cells were grown at 37 °C with shaking at 160 rpm till OD_{600} of 0.6 and were induced with 1 mM IPTG for 60 minutes prior harvesting by centrifugation at 10,000 ×g for 15 minutes at 4 °C.

Preparation of clarified lysates

Cell pellets were resuspended in 1.5 mL of cell lysis buffer (95 mM KCl, 5 mM NH_4Cl, 20 mM HEPES pH 7.5, 1 mM DTT, 5 mM $Mg(OAc)_2$, 0.5 mM $CaCl_2$, 8 mM putrescine, 1 mM spermidine, 1 tablet of cOmplete™ EDTA-free Protease Inhibitor Cocktail (Roche) per 10 mL of buffer and in the absence or presence of either 0.5 or 0.75 mM ATP), resuspended cells were opened by FastPrep homogeniser (MP Biomedicals) with 0.1 mm Zirconium beads (Techtum) in 4 cycles by 20 seconds with 1 minute chill on ice. Cell debris was removed after centrifugation at 14,800 ×g for 15 minutes at 4 °C. Total protein concentration in supernatant was measured by Bradford assay (BioRad), supernatant was aliquoted and frozen in liquid nitrogen.

Polysome fractionation and immunoblotting

Sucrose density gradient centrifugation

After melting the frozen lysates on ice, 2 A_{260} units of each extract was aliquoted into three tubes and supplemented with or without 0.5-0.75 mM ATP and was loaded onto 5–25% or 7–35% (w/v) sucrose density gradients in HEPES:Polymix buffer (Takada *et al*, 2020), 5 mM $Mg(OAc)_2$ and supplemented or not with 0.5–0.75 mM ATP. Gradients were resolved at 35,000 rpm for 2.5 hours at 4 °C in SW41 rotor (Beckman) and analysed and fractionated using Biocomp Gradient Station (BioComp Instruments) with A_{280} as a readout.

Immunoblotting

LsaA and VgaA$_{LC}$: Schleicher & Schuell Minifold II Slot Blot System SRC072/0 44-27570 Manifold was used for transferring samples from sucrose gradient fractions to PVDF membranes (Immobilon PSQ, Merk Millipore). Shortly, 15-100 μL of each sucrose gradient fraction was added to 200 μL of Slot-blotting Buffer (20 mM HEPES:KOH pH 7.5, 95 mM KCl, 5 mM NH_4Cl, 5 mM $Mg(OAc)_2$) in slots and blotted onto PVDF membrane that had been activated with methanol for one minute, wetted in MilliQ water and equilibrated with Slot-blotting Buffer (1x PM 5 mM Mg^{2+} without putrescine and spermidine) for 10 minutes. After blotting of the samples each slot was washed twice with 200 μL of Slot-blotting Buffer. The membrane was removed from the blotter, transferred to hybridization bottle, equilibrated for 10 minutes in PBS-T (1x PBS supplemented with 0.05% Tween-20) and blocked in PBS-T supplemented with 5% w/v nonfat dry milk for one hour. Antibody incubations were performed for one hour in 1% nonfat dry milk in PBS-T with five 5-minute washes in fresh PBS-T between and after antibody incubations. HTF-tagged LsaA and $FLAG_3$-tagged VgaA$_{LC}$ proteins were detected using anti-Flag M2 primary (Sigma-Aldrich, F1804; 1:10,000 dilution) antibodies

combined with anti-mouse-HRP secondary (Rockland; 610-103-040; 1:10,000 dilution) antibodies. An ECL detection was performed on ImageQuant LAS 4000 (GE Healthcare) imaging system using Pierce® ECL Western blotting substrate (Thermo Scientific). The blotting and all incubations were performed at room temperature in hybridization oven.

VgaL (Lmo0919): Western blotting of lysates on sucrose gradient fractionation was performed as previously described (Takada *et al.*, 2020). VgaL-HTF was detected using anti-Flag M2 primary (Sigma-Aldrich, F1804; 1:10,000 dilution) antibodies combined with anti-mouse-HRP secondary (Rockland; 610-103-040; 1:10,000 dilution) antibodies.

Affinity purification on anti-FLAG M2 affinity gel

100 µL of well mixed anti-FLAG M2 Affinity Gel aliquots were loaded on columns (Micro Bio-Spin Columns, Bio-Rad) and washed two times with 1 mL of cell lysis buffer by gravity flow. All incubations, washings and elutions were done at 4 °C.

The total protein concentration of each lysate was adjusted to 2 mg/mL with cell lysis buffer and 1 mL of each lysate was loaded on columns and incubated for two hours with end-over-end mixing for binding. The columns were washed 5 times by 1 mL of cell lysis buffer by gravity flow. For elution of FLAG-tagged proteins and their complexes 100-300 µL of 0.1 mg/mL $FLAG_3$ peptide (Sigma) was added to samples, the solutions were incubated at 4 °C for 20 minutes with end-over-end mixing. Elutions were collected by centrifugation at 2,000 ×g for 2 minutes at 4 °C.

20 µL aliquots of collected samples (flow-through, washes and elutions) were mixed with 5 µL of 5x SDS loading buffer and heated up at 95 °C for 15 minutes. The beads remaining in the column were washed twice with 1 mL of cell lysis buffer and resuspended in 100 µL of 1x SDS loading buffer. Denatured samples were resolved on 12-15% SDS-PAGE. SDS-gels were stained by “Blue-Silver” Coomassie Staining (Candiano *et al*, 2004) and washed with water for 6 hours or overnight before imaging with LAS4000 (GE Healthcare).

tRNA microarrays

To fully deacylate tRNAs, eluates and input lysate samples from two biological replicates were mixed with 80 µL 250 mM Tris-HCl, pH 9.0, 10 µL 0.2 M EDTA, 10 µL 1% SDS, and incubated for 45 min, and neutralised with 200 µL 1 M NaOAc, pH 5.5, before mixing 1:1 with acidic phenol:chloroform alcohol 5:1. The supernatant was precipitated with ethanol and dissolved in ddH_2O.

tRNA microarrays were performed as described (Kirchner *et al*, 2017). Briefly, using the unique invariant single stranded 3′-NCCA-ends of intact tRNA a Cy3-labelled or Atto647-labeled RNA/DNA hybrid oligonucleotide was ligated to the tRNA extracted from the RqcH-50S samples and total *E. faecalis* tRNA (from the lysate), respectively. Labeled tRNA was purified by phenol:chloroform extraction and loaded on a microarray containing 24 replicates of full-length tDNA probes recognizing *E. faecalis* tRNA isoacceptors. Florescence signals were normalized to three *in vitro* transcribed human tRNAs, spiked in to each sample. Microarrays were statistically analysed with in-house scripts written in Python 3.7.0.

Grid preparation, cryo-electron microscopy and single-particle reconstruction

Preparation of cryo-EM grids and data collection

Elutions from LsaA and VgaL pull-downs were loaded on grids within two hours after obtaining them without freezing, samples were kept on ice. The $VgaA_{LC}$ sample was frozen in liquid nitrogen after pull-down, defrosted and loaded later. After glow-discharging of grids, 3.5 mL of sample was loaded on grids in Vitrobot (FEI) in conditions of 100% humidity at 4 °C, blotted for 5 seconds and vitrified by plunge-freezing in liquid ethane. Samples were imaged on a Titan Krios (FEI) operated at 300 kV at a nominal magnification of 165 k× (0.86 Å/pixel, later estimated to be 0.82 Å/pixel by comparing refined maps to structures with known magnification) with a Gatan K2 Summit camera at an exposure rate of 5.80 electrons/pixel/s with a 4 seconds exposure and 20 frames using the EPU software. Quantifoil 1.2/1.3 Cu_{200} grids were used for LsaA and $VgaA_{LC}$ and Quantifoil 2/2 Cu_{200} grids were used for VgaL.

Single-particle reconstruction

Motion correction was performed with MotionCor2 with 5×5 patches (Zheng *et al*, 2017). Relion 3.0 or 3.1 was used for further processing unless otherwise stated and resolutions are reported according to the so-called ‘gold standard’ criteria (Henderson *et al*, 2012; Scheres & Chen, 2012; Zivanov *et al*, 2018). CTFFIND4 (LsaA dataset) or Gctf v1.06 ($VgaA_{LC}$ and VgaL datasets) was used for CTF estimation (Rohou & Grigorieff, 2015; Zhang, 2016). Particles were picked with Gautomatch (https://www2.mrc-lmb.cam.ac.uk/research/locally-developed-software/zhang-software/#gauto, developed by K. Zhang) without supplying a reference, and in the case of LsaA, re-picked using RELION autopicker after templates were generated by 2D classification. Particles were initially extracted at 2.46 Å/pixel and subjected to 2D classification. Classes that resembled ribosomes were used for 3D refinement, with a 60 Å low-pass filter applied to initial references. For 3D refinement of LsaA–70S, the initial reference was EMDB-0176, a *B. subtilis* 70S ribosome with no factor bound in the E-site (Crowe-McAuliffe *et al.*, 2018); for $VgaA_{LC}$–70S and VgaL–70S 3D refinements the RELION initial

model job type was used to create a reference from particles selected after 2D classification. 3D classification was performed without angular sampling, and classes of interest were re-extracted at 0.82 Å/pixel for further refinement.

In the case of LsaA, after initial 3D classification, a soft mask around the A-site was used for partial signal subtraction followed by focussed classification. The classes with the strongest and weakest A-site density were selected for signal restoration and refinement. In the case of the $VgaA_{LC}$ dataset, initial 3D classification yielded a class with apparent sub-stoichiometric density in the E-site corresponding to $VgaA_{LC}$. Micrographs with poor values from CTF estimation were discarded, particles were re-extracted, subjected to an additional 2D classification and 3D refinement, followed by Bayesian polishing and CTF refinement. An additional 3D classification yielded a class with strong E-site density corresponding to the factor. Refer to Figures S4–S6 for details.

For multibody refinements, soft masks around the small subunit body, small subunit head, and large subunit/ARD were applied. In the case of the $VgaA_{LC}$ dataset, particles were first re-extracted in a smaller box (360×360 pixels) and subjected to 3D refinement prior to multibody refinement.

ResMap was used to estimate local resolution (Kucukelbir *et al*, 2014). Maps were locally filtered using SPHIRE (Moriya *et al*, 2017).

Molecular modelling

For the *E. faecalis* and *L. monocytogenes* ribosomes, homology models were generated with SWISS-MODEL (Waterhouse *et al*, 2018), mostly from PDB 6HA1/6HA8 (Crowe-McAuliffe *et al.*, 2018). PDBs 4YBB (Noeske *et al*, 2015) 5MDV (James *et al*, 2016) were used as additional templates and references where necessary, 4V9O (Pulk & Cate, 2013) was used for bS21, 5ML7 (Gabdulkhakov *et al*, 2017) and 3U4M (Tishchenko *et al*, 2012) were used for the L1 stalk region, 5AFI (Fischer *et al*, 2015) and 5UYQ (Loveland *et al*, 2017) were used for tRNAs, and 6QNQ was used to help placing metal ions (Rozov *et al*, 2019). PDB 5LI0 (Khusainov *et al.*, 2016) was used as a starting model for the *S. aureus* ribosome. Where appropriate, individual components of multibody refinements were fitted into density from the corresponding locally filtered map to help modelling. Models were adjusted with Coot (Casañal *et al*, 2020) and refined using locally filtered maps in Phenix version 1.14 3260 (Liebschner *et al*, 2019).

Figures were created with PyMOL 2.0 (Schrödinger, LLC), UCSF Chimera (Pettersen *et al*, 2004), RELION (Zivanov *et al.*, 2018), and Igor Pro (WaveMetrics, Inc.). Structures were aligned in PyMOL using the 23S rRNA unless otherwise noted.

Figures were assembled with Adobe Illustrator (Adobe Inc.).

Supplementary Material

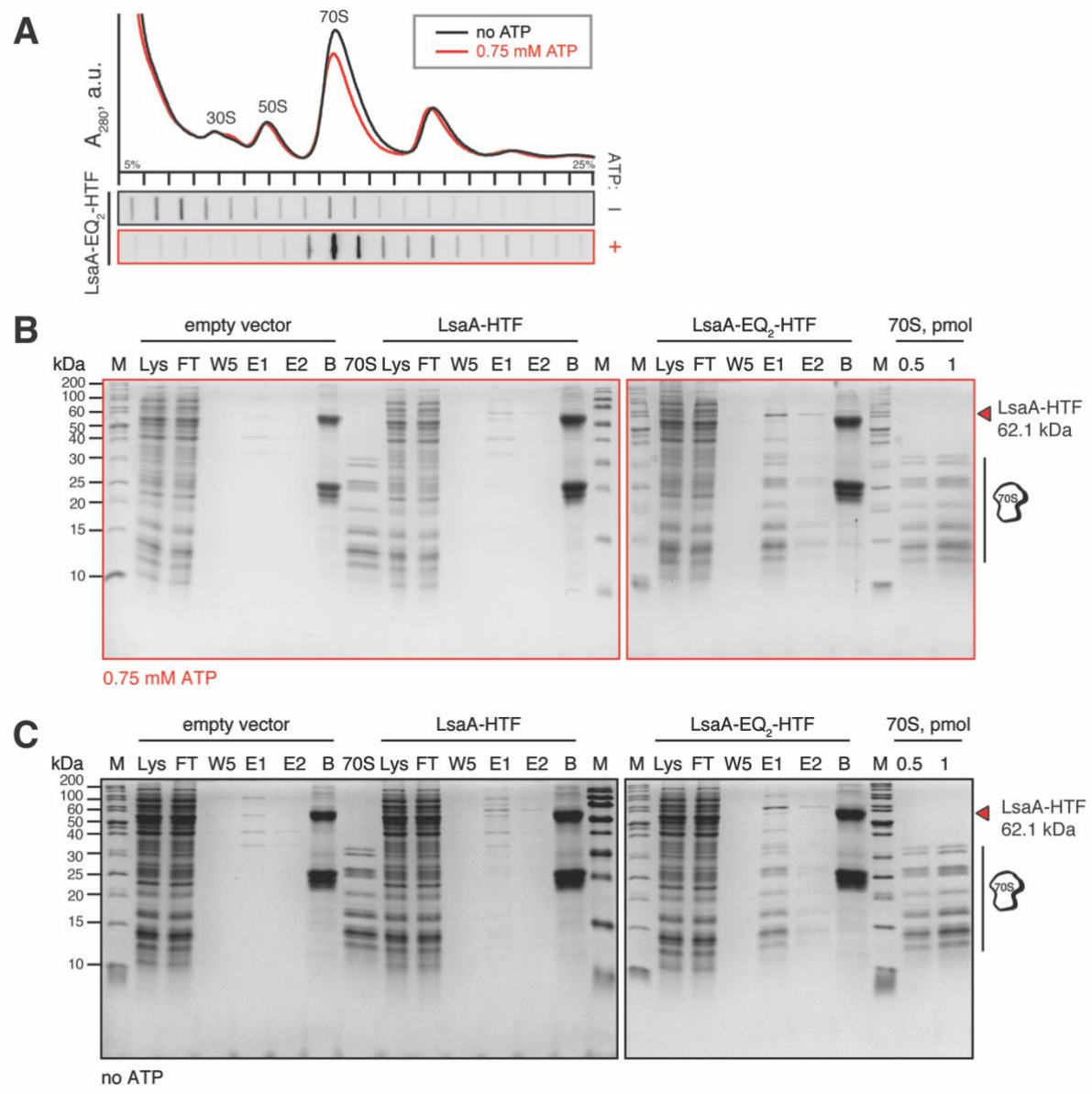

Figure S1. Characterization of *E. faecalis* LsaA interactions with ribosomes and preparation of samples for cryo-EM. (**A**) Polysome profiles and immunoblot analyses of C-terminally His_6-TEV-$FLAG_3$-tagged (HTF) ATPase-deficient (EQ_2) LsaA-EQ_2 ectopically expressed in Δ*lsaA E. faecalis* TX5332. Experiments were performed both in the presence or absence of 0.75 mM ATP in gradients. (**B, C**) Affinity purification of wild-type and EQ_2 *E. faecalis* LsaA-HTF ectopically expressed in TX5332 *E. faecalis*. Pull-down experiments were performed either in the presence (**B**) or absence (**C**) of 0.75 mM ATP using clarified lysates of *E. faecalis* either transformed with empty pCIE vector (background control), expressing *E. faecalis* LsaA-HTF (VHp100) or expressing *E. faecalis* LsaA-EQ_2-HTF (VHp149). Samples: M: molecular weight marker; Lys: 2 µL of clarified lysate, FT: 2 µL of

flow-through; W5: 10 µL of last wash before specific elution; E1: 10 µL of the first elution with $FLAG_3$ peptide; E2: 10 µL of the second elution with $FLAG_3$ peptide; B: 10 µL of SDS-treated post-elution anti-FLAG beads; 70S: purified *E. faecalis* 70S ribosomes. The samples were resolved on 15% SDS-PAGE gel. The 0.75 mM ATP *E. faecalis* LsaA-EQ_2-HTF pulldown sample was used for further cryo-EM and tRNA array analysis.

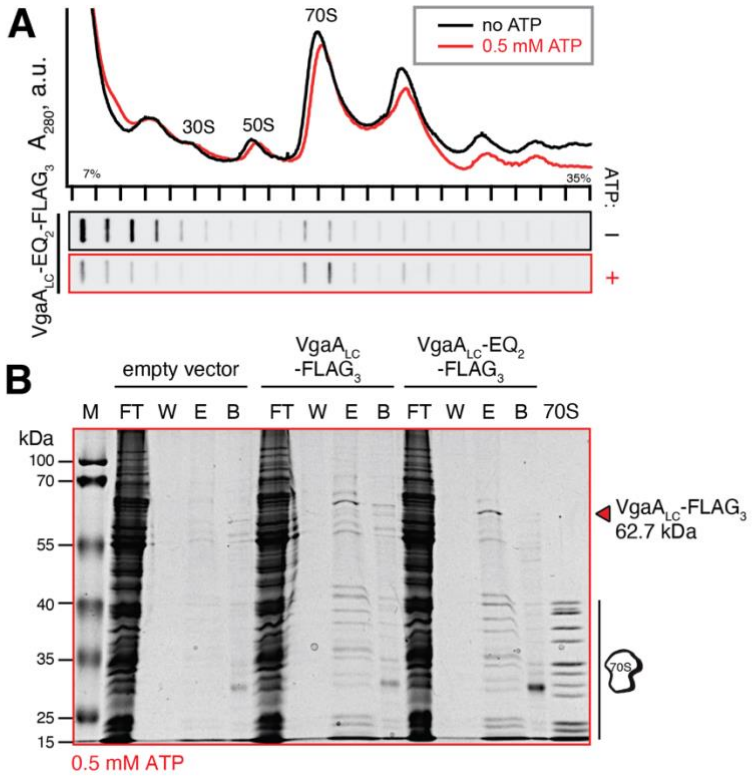

Figure S2. Characterization of *S. haemolyticus* VgaA$_{LC}$ interactions with ribosomes and reparation of samples for cryo-EM reconstructions. (**A**) Polysome profiles and immunoblot analyses of FLAG$_3$-tagged *S. haemolyticus* VgaA$_{LC}$-EQ$_2$ ectopically expressed in wild-type SH-1000 *S. aureus*. Experiments were performed both in the presence or absence of 0.5 mM ATP in gradients. (**B**) Affinity purification of wild-type and EQ$_2$ *S. haemolyticus* VgaA$_{LC}$-FLAG$_3$ ectopically expressed in SH-1000 *S. aureus*. Immunoprecipitations were performed in the presence of 0.5 mM ATP and the samples were resolved on a 15% polyacrylamide gel by SDS-PAGE. Samples: M: 2 µL of molecular weight marker; FT: 2 µL of flow-through, W: 10 µL of last wash before specific elution; E: 10 µL of elution with FLAG$_3$ peptide; B: 2 µL of SDS-treated post-elution anti-FLAG beads; 70S: 1 pmol of purified *S. aureus* 70S ribosomes. The 0.5 mM ATP *S. haemolyticus* VgaA$_{LC}$-EQ$_2$-HTF pulldown sample was used for cryo-EM reconstructions.

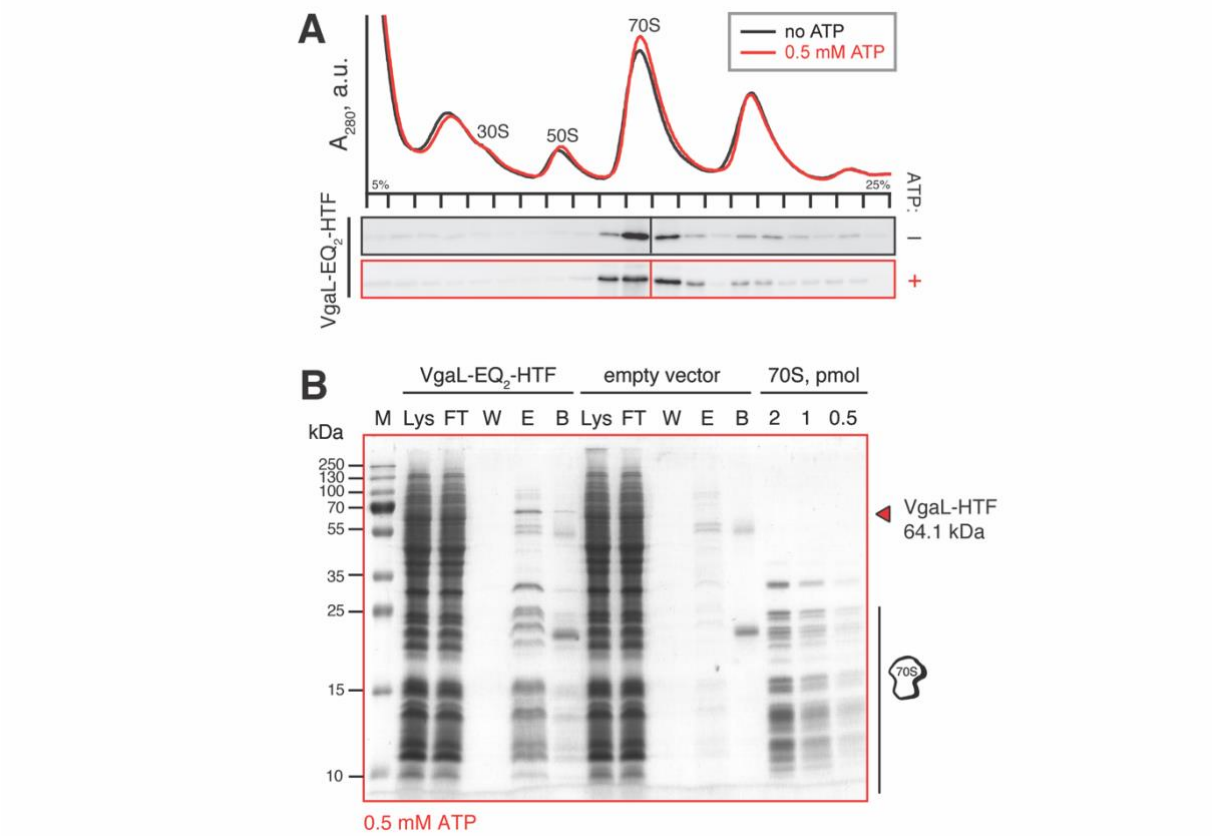

Figure S3. Characterization of *L. monocytogenes* VgaL (Lmo0919) interactions with ribosomes and reparation of samples for cryo-EM reconstructions. (**A**) Polysome profiles and immunoblot analyses of HTF-tagged *L. monocytogenes* VgaL-EQ_2 (Lmo0919-EQ_2) ectopically expressed in wild-type EDG-*e L. monocytogenes*. Experiments were performed both in the presence or absence of 0.5 mM ATP in gradients. (**B**) Affinity purification of *L. monocytogenes* VgaL-EQ_2 ectopically expressed in EDG-*e L. monocytogenes*. Pull-down experiments were performed in the presence of 0.5 mM ATP using clarified lysates of *L. monocytogenes* transformed with empty integrative pIMK3 vector (background control), expressing VgaL-HTF (VHp692) or expressing VgaL-EQ_2-HTF (VHp149). Samples: M: 2 µL of molecular weight marker; FT: 2 µL of flow-through; W: 10 µL of last wash before specific elution; E: 10 µL of elution with $FLAG_3$ peptide; B: 2 µL of SDS-treated post-elution anti-FLAG beads; 70S: purified *B. subtilis* 70S ribosomes, the samples were resolved on 15 % SDS-PAGE gel. The 0.5 mM ATP *L. monocytogenes* VgaL-EQ_2-HTF pulldown sample was used for cryo-EM reconstructions.

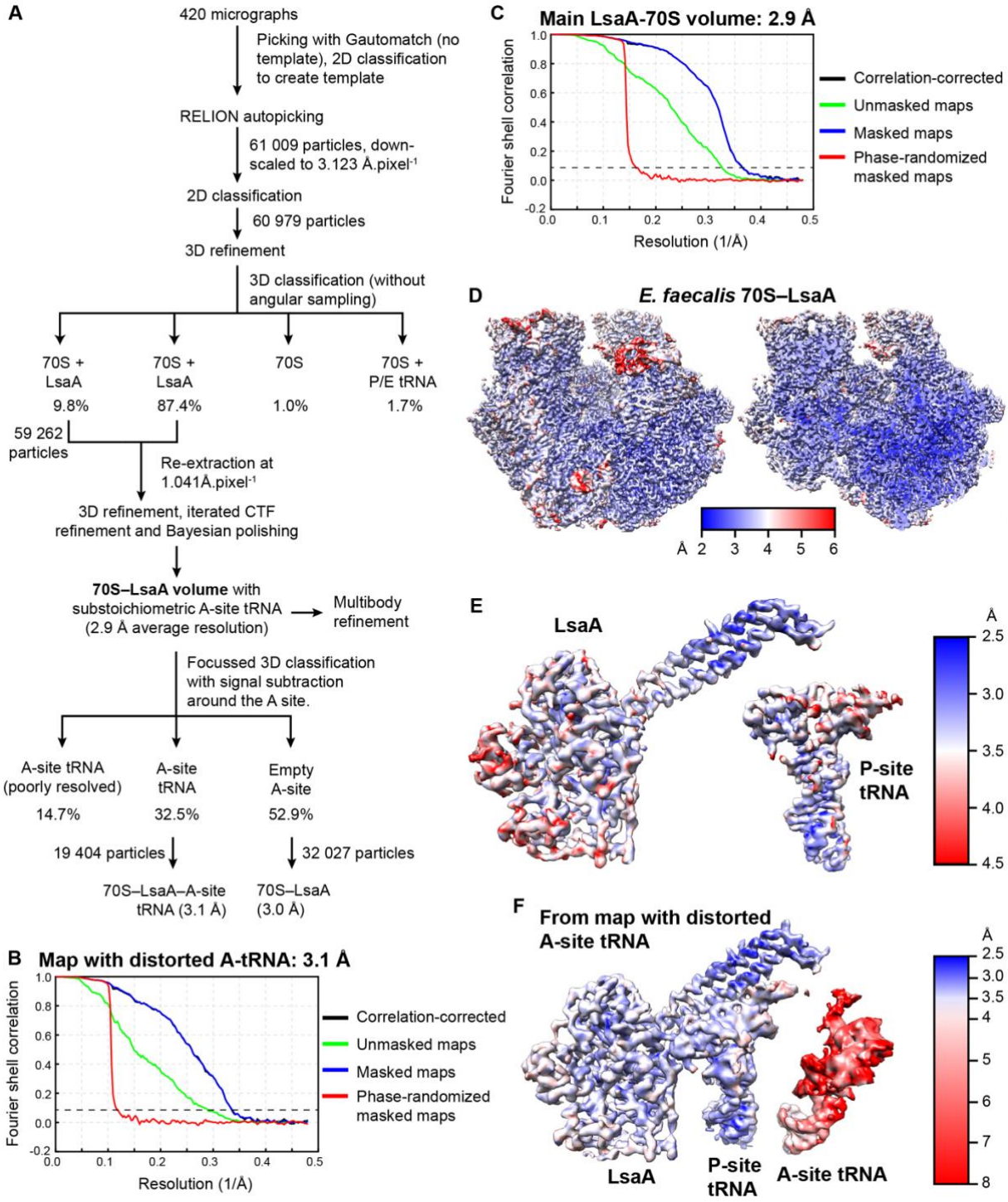

Figure S4. Processing of the cryo-EM data of LsaA-70S complex. (**A**) Processing scheme for the LsaA-70S complex, yielding two subpopulations of LsaA-70S complexes with and without A-site tRNA. (**B, C**) Fourier Shell Correlation (FSC) curves of the LsaA-70S (**B**) with A-tRNA and (**C**) without A-tRNA with a dashed line at 0.143 indicating average resolutions of 3.1 Å and 2.9 Å, respectively. (**D**) Overview (left) and transverse section (right) of the cryo-EM map of the LsaA-70S (without A-tRNA) coloured according to local resolution. (**E**) Isolated density of LsaA (left) and P-site tRNA (right) from (D). (**F**) Isolated density of LsaA, P-site and A-site tRNA from the LsaA-70S map (with A-tRNA) coloured according to local resolution.

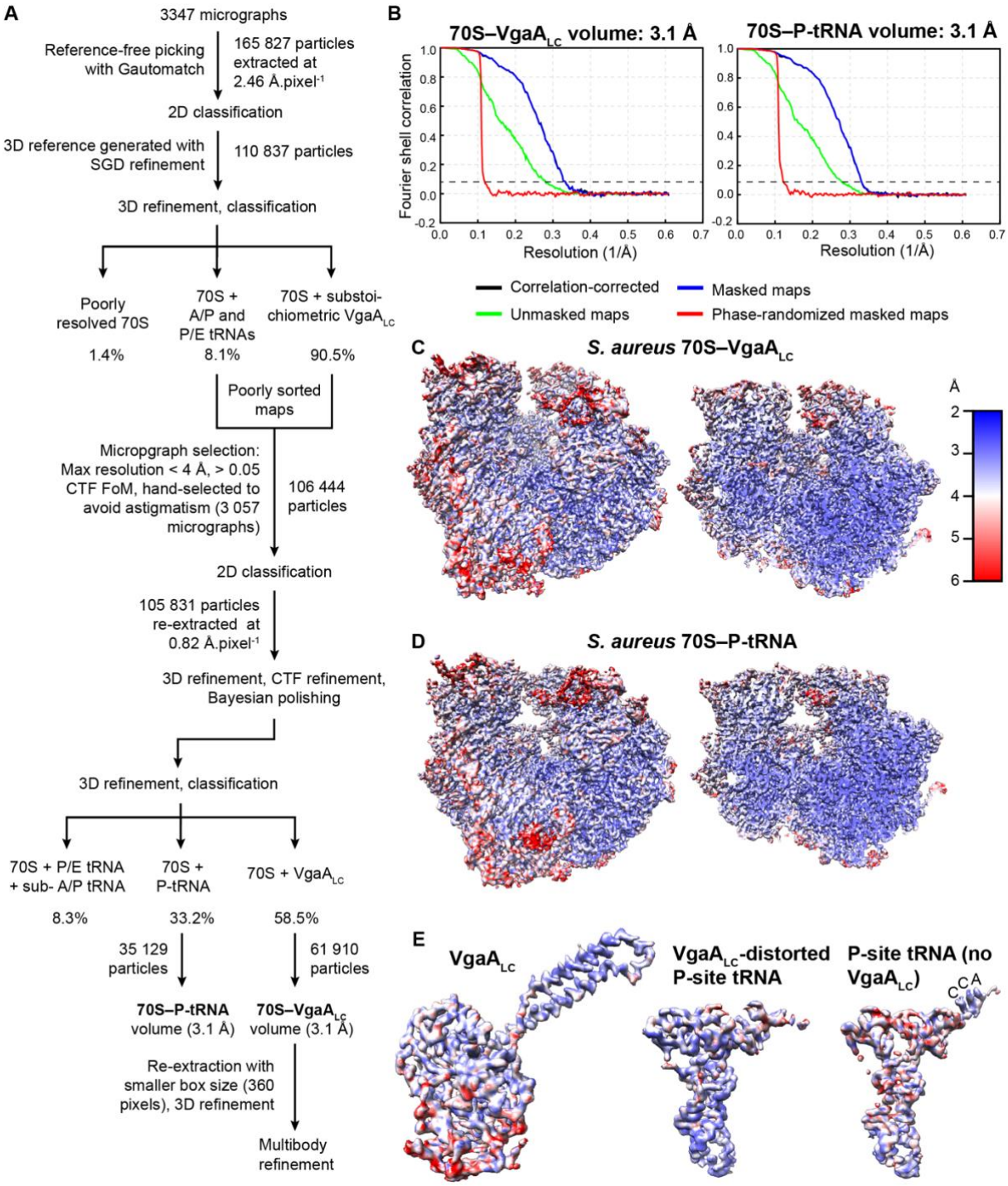

Figure S5. Processing of the cryo-EM data of VgaA$_{LC}$–70S complex. (**A**) Processing scheme for the LsaA-70S complex, yielding a VgaA$_{LC}$–70S and 70S–P-tRNA complex without VgaA$_{LC}$. (**B**) Fourier Shell Correlation (FSC) curves of the VgaA$_{LC}$–70S and 70S–P-tRNA complexes with a dashed line at 0.143 indicating average resolutions of 3.1 Å. (**C, D**) Overview (left) and transverse section (right) of the cryo-EM map of the (**C**) VgaA$_{LC}$–70S and (**D**) 70S-P-tRNA complexes coloured according to local resolution. (**E**) Isolated density of VgaA$_{LC}$ (left) and P-site tRNA (right) from the VgaA$_{LC}$–70S complex, and the P-site-tRNA from the 70S–P-tRNA complex, coloured according to local resolution.

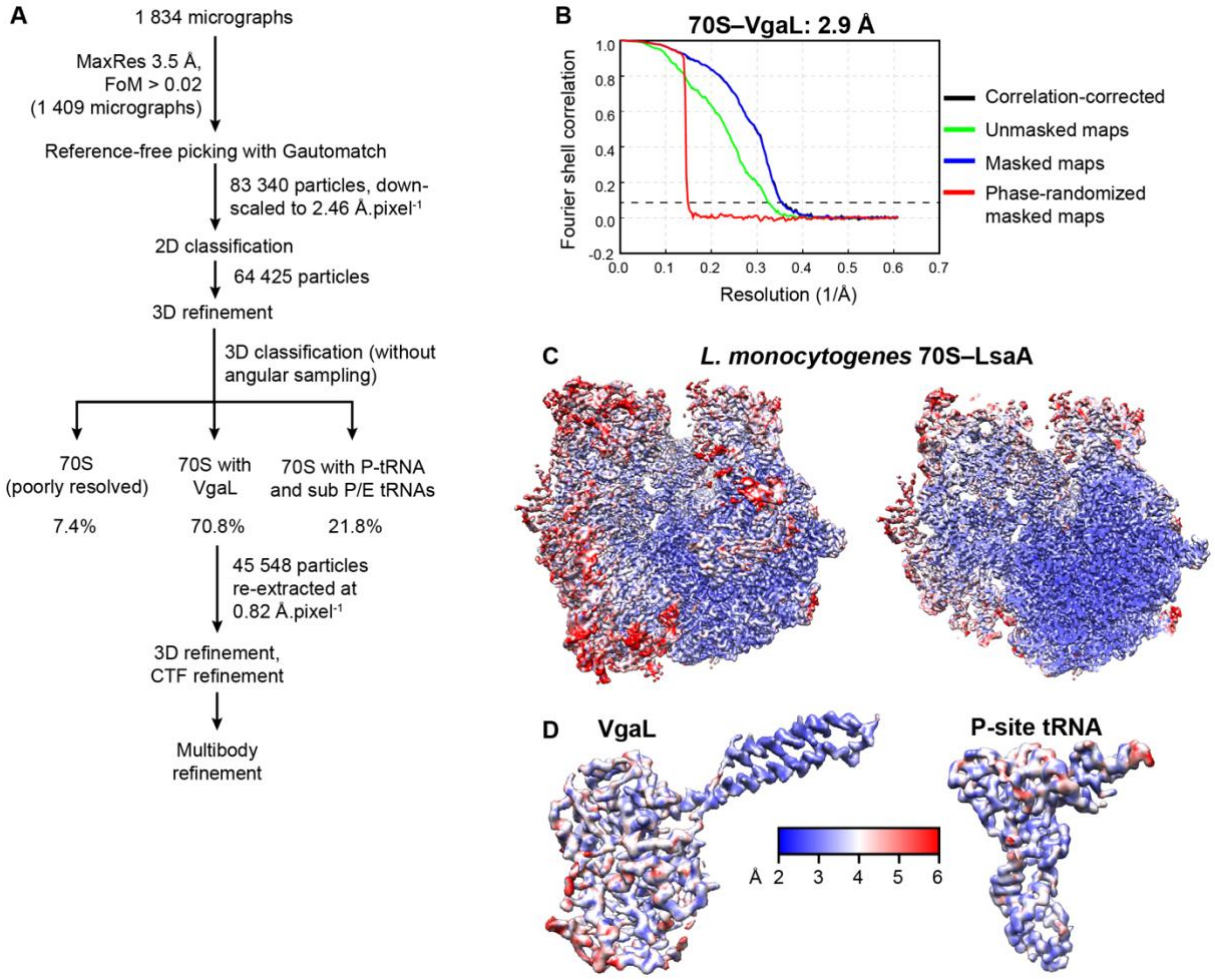

Figure S6. Processing of the cryo-EM data of VgaL–70S complex. (**A**) Processing scheme for the VgaL–70S complex. (**B**) Fourier Shell Correlation (FSC) curves of the VgaL-70S complex with a dashed line at 0.143 indicating average resolutions of 2.9 Å. (**C**) Overview (left) and transverse section (right) of the cryo-EM map of the VgaL–70S complex coloured according to local resolution. (**D**) Isolated density of VgaL (left) and P-site tRNA (right) from the VgaL-70S complex coloured according to local resolution.

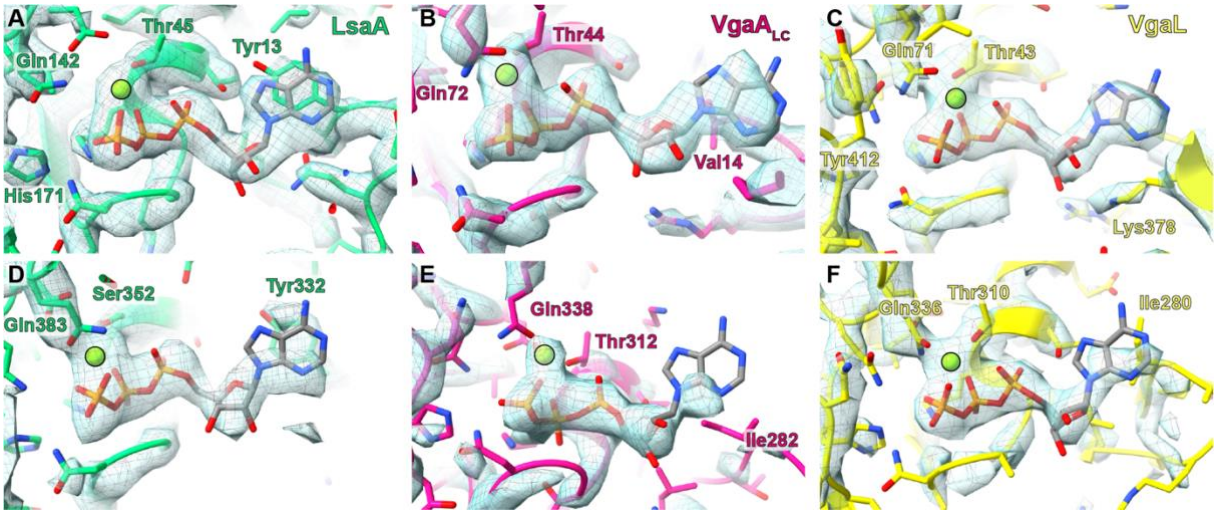

Figure S7. ATP in the ARE-bound 70S structures. Model and density surrounding the innermost ATP bound by LsaA (**A**), $VgaA_{LC}$ (**B**), and VgaL (**C**) viewed from the direction of the signature sequence of NBD2 (model and density not shown). A black outline highlights a magnesium ion. **D–F**, as for **A–C** except for the peripheral nucleotide-binding site viewed from the direction of the signature sequence of NBD1 (model and density not shown). Density from post-processed maps is shown.

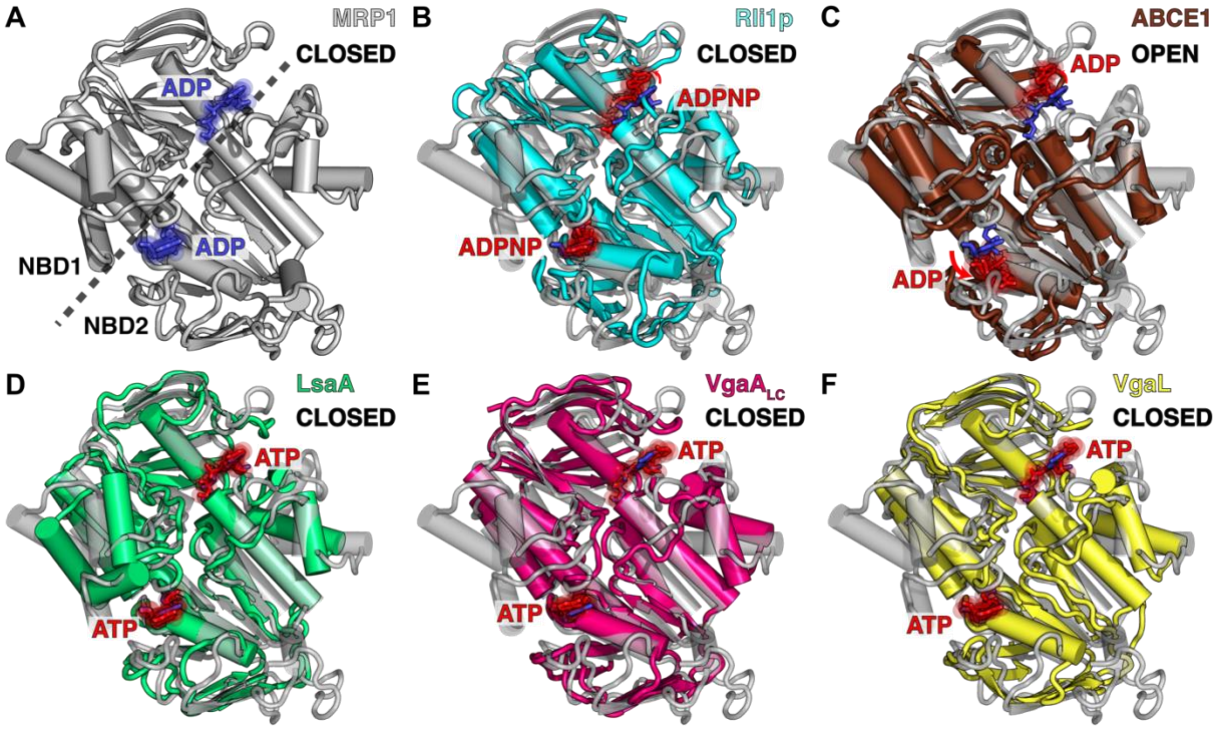

Figure S8 LsaA, VgaA$_{LC}$ and VgaL NBDs exhibit a closed conformation. (**A**) The closed conformation of the multidrug transporter MRP1 (grey) with bound ADP molecules (blue, PDB 6BHU) (Johnson & Chen, 2018). (**B, C**) Alignment (based on NBD1) and superimposition of the closed conformation of MRP1 from (**A**) with the ABC domains of (**B**) Rli1p (cyan) in closed conformation with bound ADPNP (red, PDB 5LL6) (Heuer *et al*, 2017), (**C**) ABCE1 (brown) in open conformation with bound ADP (red, PDB 3J15) (Becker *et al*, 2012), and with (**D–F**) closed ARE ABCF NBD conformations with bound ATP (red) for (**D**) LsaA (green), (**E**) VgaA$_{LC}$ (magenta) and (**F**) VgaL (yellow).

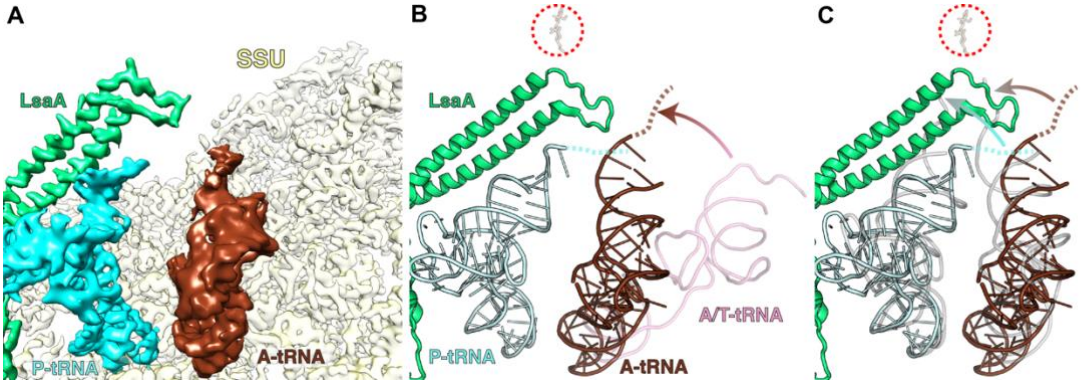

Figure S9. Presence of A-site tRNA in the LsaA-70S complex. (**A**) Cryo-EM map density for LsaA (green), P-site tRNA (cyan) and A-site tRNA (brown) in the LsaA–70S complex with A-site tRNA. Density for small subunit (yellow) is shown for reference. Density for the large subunit is not shown. (**B**) The same view as A, except with molecular models. The brown dashed line indicates a likely path for the 3′ CCA end of the distorted A-tRNA. A pre-accommodation A/T tRNA (pink, PDB 4V5L) (Voorhees *et al*, 2010) is superimposed. The position of the lincomycin binding site (red dotted circle) is shown for comparison (PDB 5HKV) (Matzov *et al.*, 2017). (**C**) Similar to (**B**) except with classical accommodated A- and P-site tRNAs from pre-attack state superimposed (both grey, PDB 1VY4) (Polikanov *et al.*, 2014).

1491

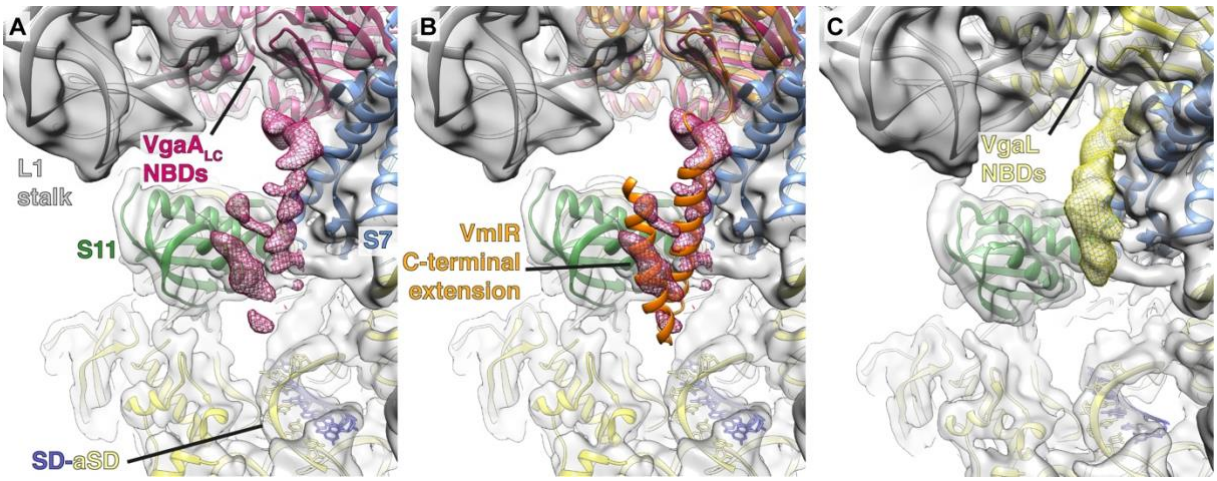

1492

1493 **Figure S10. C-terminal extensions of VgaA$_{LC}$ and VgaL on the small subunit.** (**A-C**)
1494 Cryo-EM map (grey) with molecular model for (**B–C**) VgaA$_{LC}$–70S complex, and (**C**) VgaL–
1495 70S complex, showing density for L1 stalk (grey) on the large subunit, and ribosomal
1496 proteins S7 (blue), S11 (green) as well as the SD–anti-SD helix on the small subunit (yellow).
1497 In (**A**) and (**B**), density for the C-terminal extension (CTE) of VgaA$_{LC}$ (magenta mesh) is
1498 fragmented, and in (**B**) fitted with the model of the CTE from VmlR (orange, PDB 6HA8)
1499 (Crowe-McAuliffe *et al.*, 2018) based on alignment of the NBDs. In (**C**), density for the C-
1500 terminal extension (CTE) of VgaL (yellow mesh) also reaches between the S7–S11 cleft and
1501 is consistent with an α-helical conformation, but appears to be distinct from VmlR and
1502 VgaA$_{LC}$ and could not be modelled at this resolution.

1503

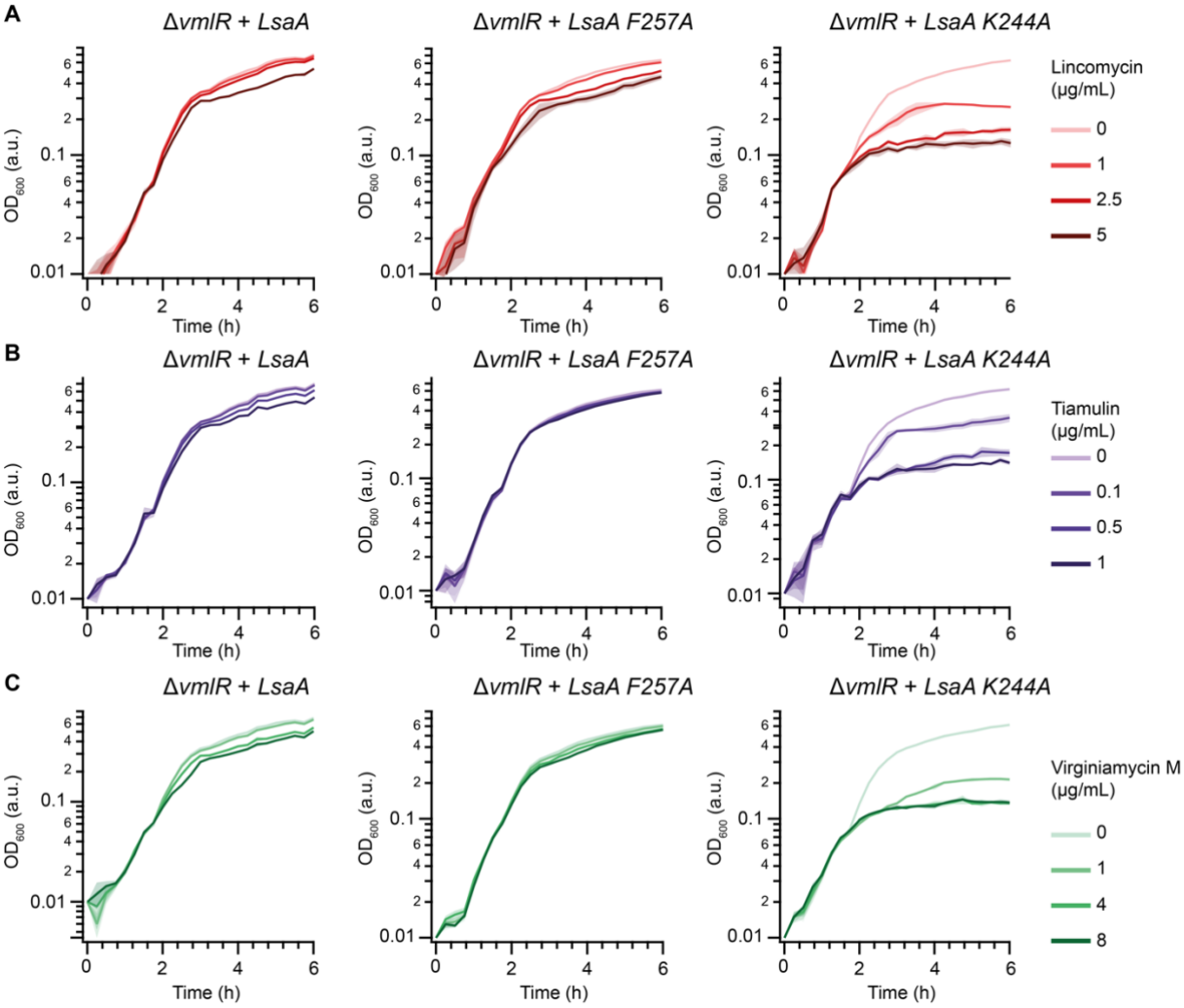

Figure S11. Effect of amino acid substitutions in ARD on antibiotic resistance in LsaA. Growth of *B. subtilis* Δ*vmlR* expressing the indicated LsaA variants over time in the presence of lincomycin (**A**), tiamulin (**B**), and virginiamycin M (**C**). *B. subtilis* strains (VHB109, 168 and 169) were grown in LB media with 1 mM IPTG at 37 °C with medium shaking. At the 90 minutes time point (OD_{600} ≈ 0.1) antibiotics were added to the final concentrations as indicated on the figure. The SD of three biological replicates is indicated with pale shading.

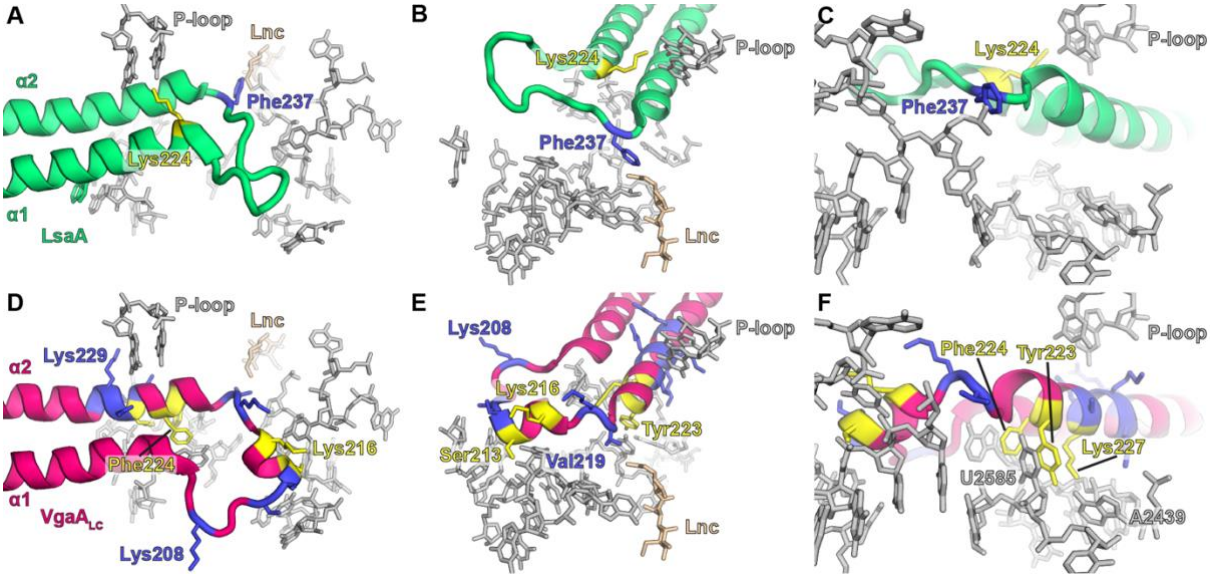

Figure S12. Visualisation of tested mutations in $VgaA_{LC}$ and LsaA. Residues in blue did not affect antibiotic resistance when mutated to alanine, and residues in yellow reduced antibiotic resistance when mutated to alanine. **A–C**, three views of the LsaA ARD with selected *E. faecalis* 23S 23S rRNA nucleotides shown. **D–F**, three views of the $VgaA_{LC}$ ARD with selected *S. aureus* 23S 23S rRNA nucleotides shown. See also Tables S1 and S2.

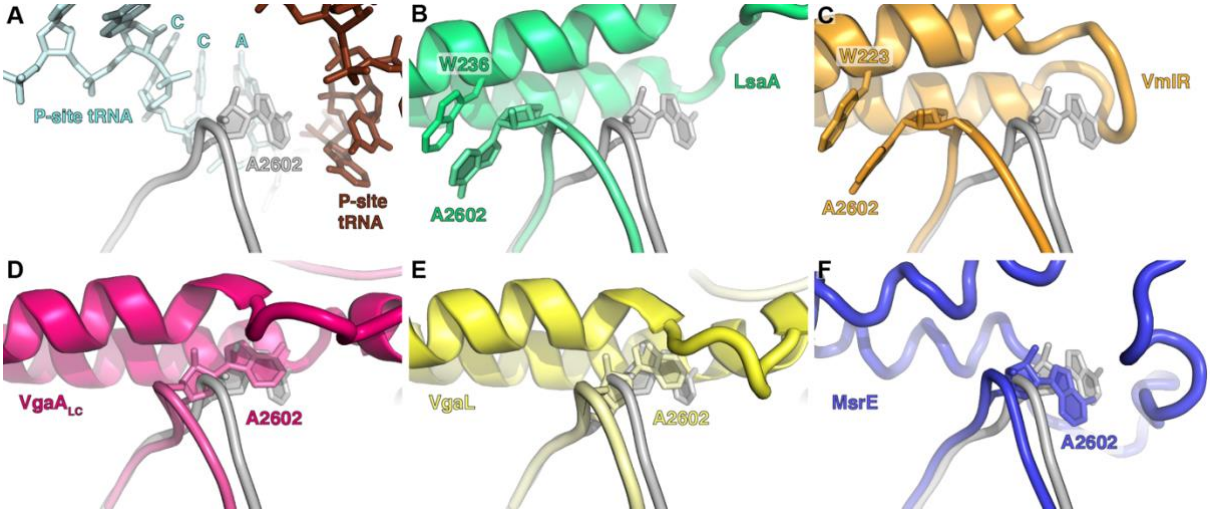

Figure S13. Comparison of A2602 position between ribosomes with and without bound AREs. (**A**) A2602 with accommodated A- and P-site tRNAs in the 'pre-attack' state (PDB 1VY4) (Polikanov *et al.*, 2014) (**B**) Conformation of A2602 with bound LsaA with 23S rRNA from (**A**). (**C–F**) Similar to (**B**), except for VmlR, VgaA$_{LC}$, VgaL, and MsrE (Crowe-McAuliffe *et al.*, 2018; Su *et al.*, 2018).

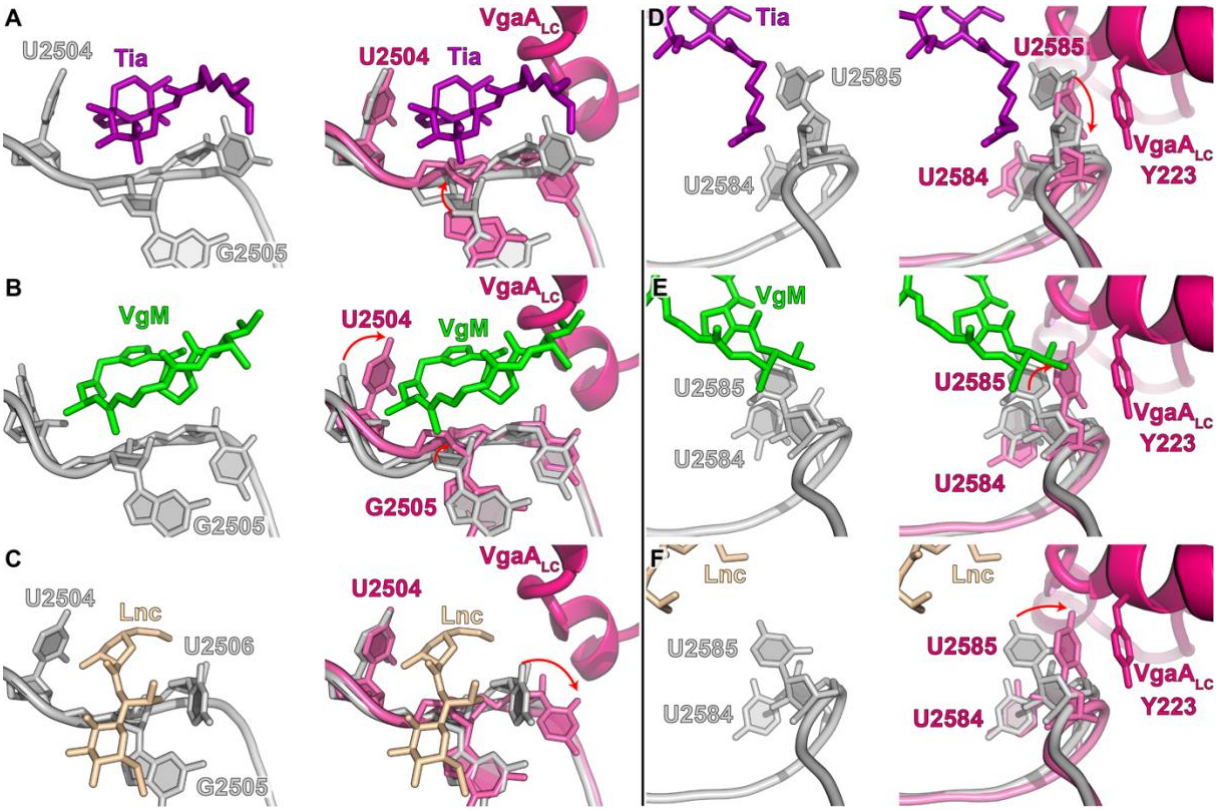

Figure S14. Conformation of the PTC in the presence of VgaA$_{LC}$ and antibiotics. (**A–C**) The conformation of selected 23S rRNA nucleotides at the PTC in the presence of either (**A**) tiamulin (Tia, purple, PDB 1XBP) (Schlünzen *et al.*, 2004), (**B**) virginiamycin M (VgM, green, PDB 1YIT) (Tu *et al.*, 2005), or (**C**) lincomycin (Lnc, tan, PDB 5HKV) (Matzov *et al.*, 2017). Left panels show the antibiotic-bound structures only, right panels have superimposed nucleotides and protein from the VgaA$_{LC}$-bound ribosome (pink). (**D–F**) As for A–C, except with focus on U2585. Red arrows indicate significant shifts in nucleotide positions from antibiotic-bound to VgaA$_{LC}$-bound ribosomes.

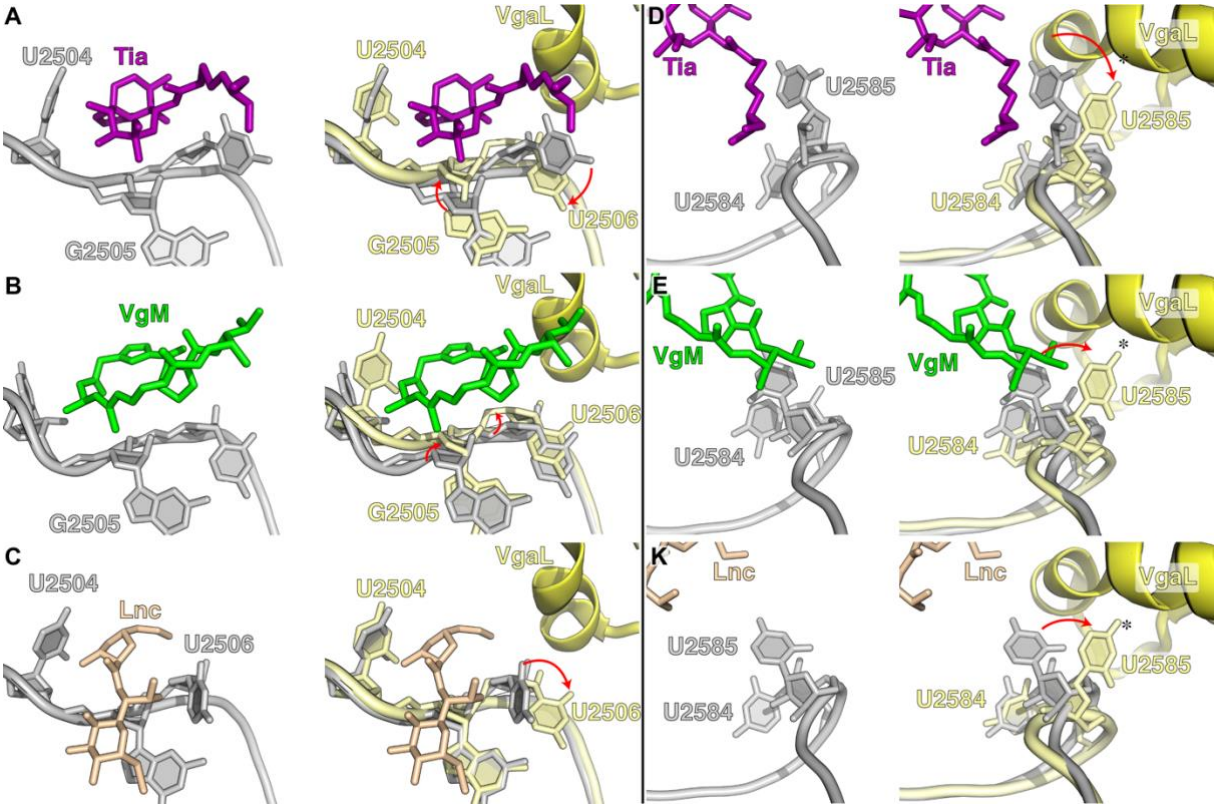

Figure S15. Conformation of the PTC in the presence of VgaL and antibiotics. The conformation of selected 23S rRNA nucleotides at the PTC in the presence of either (**A**) tiamulin (Tia, purple, PDB 1XBP) (Schlünzen *et al.*, 2004), (**B**) virginiamycin M (VgM, green, PDB 1YIT) (Tu *et al.*, 2005), or (**C**) lincomycin (Lnc, tan, PDB 5HKV) (Matzov *et al.*, 2017). Left panels show the antibiotic-bound structures only, right panels have superimposed nucleotides and protein from the VgaL-bound ribosome (yellow). (**D–F**) As for **A**–**C**, except with focus on U2585. Red arrows indicate significant shifts in nucleotide positions from the antibiotic-bound to VgaL-bound ribosome. An asterisk indicates low confidence in the position of U2585 due to weak density.

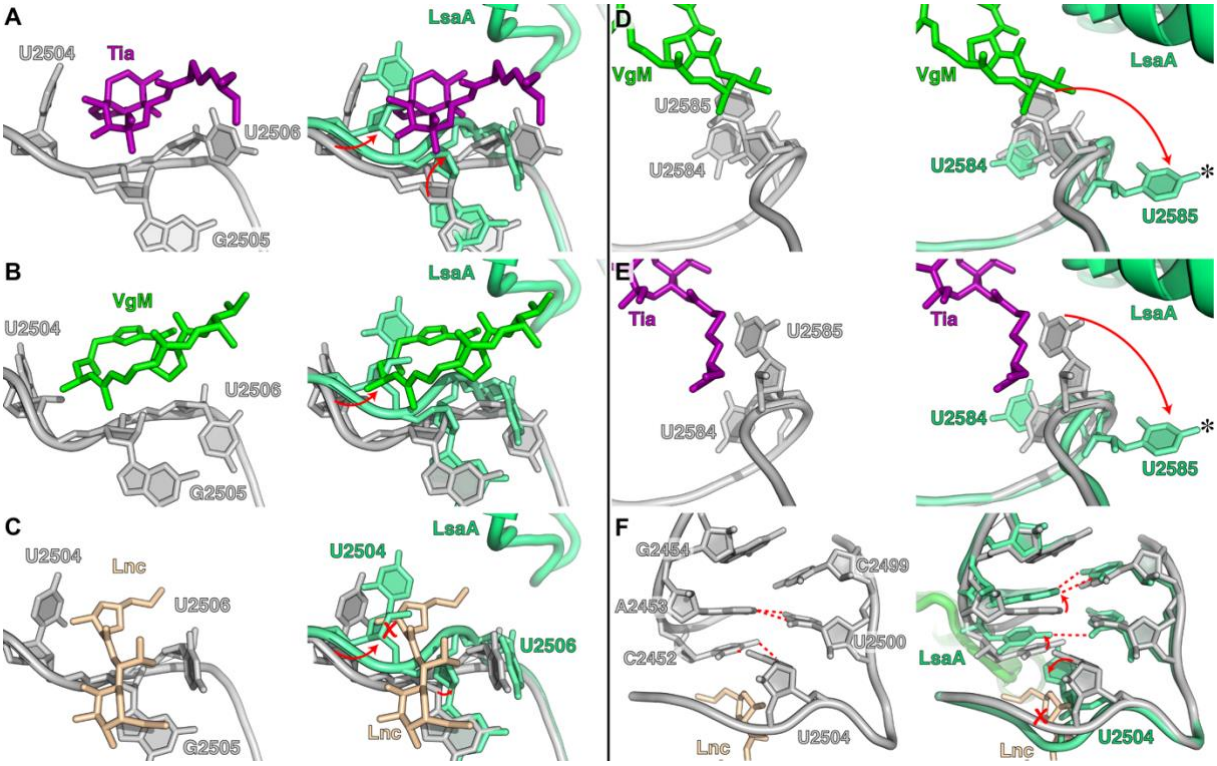

Figure S16. Conformation of the PTC in the presence of LsaA and antibiotics. (**A–C**) The conformation of selected 23S rRNA nucleotides at the PTC in the presence of either (**A**) tiamulin (Tia, purple, PDB 1XBP) (Schlünzen *et al.*, 2004), (**B**) virginiamycin M (VgM, green, PDB 1YIT) (Tu *et al.*, 2005), or (**C**) lincomycin (Lnc, tan, PDB 5HKV) (Matzov *et al.*, 2017). Left panels show the antibiotic-bound structures only, right panels have superimposed nucleotides and protein from the LsaA-bound ribosome (green). (**D–F**) As for A–C, except with focus on U2585 (**D**, **E**) or U2504 (**F**). Red arrows indicate significant shifts in nucleotide positions from antibiotic-bound to LsaA-bound ribosomes, and red crosses indicate significant overlap between the lincomycin-binding site and U2504 in the LsaA-bound ribosome. An asterisk indicates low confidence in the position of U2585 due to weak density.

Table S1. Minimum inhibitory concentrations (MICs) of ribosome-targeting antibiotics against *E. faecalis* expressing LsaA. 5 x 10^5 CFU/mL (OD_{600} approximately 0.0005) of either *E. faecalis* OG1RF, Δ*lsaA* (*lsa::Kan*) strain TX5332 transformed with empty $pCIE_{spec}$ plasmid, or with $pCIE_{spec}$ derivative for expression of LsaA was used to inoculate BHI media supplemented with 2 mg/mL kanamycin to prevent *lsa* revertants, 0.1 mg/mL spectinomycin to maintain the $pCIE_{spec}$ plasmid, 100 ng/mL of cCF10 peptide to induce expression of LsaA as well as increasing concentrations of antibiotics. After 16-20 hours at 37 °C without shaking, the presence or absence of bacterial growth was scored by eye. The MIC values that exceed the empty vector control are shown in bold.

		MIC, µg/mL			
antibiotic class	antibiotic	*E. faecalis* OG1RF	*E. faecalis* TX5332 $pCIE_{spec}$ (VHp426)	*E. faecalis* TX5332 $pCIE_{spec}$ *lsaA* (VHp431)	*E. faecalis* TX5332 pCIE *lsaA*-*HTF*
phenicols	chloramphenicol	2-4	2-4	2-4	
	thiamphenicol	4	4	4	
	florfenicol	1	1-2	1-2	
oxazolidinones	linezolid	1	1	1	1
macrolides	erythromycin	1	0.5-1	0.5	0.5
	azithromycin	1-2	0.5-1	0.5-1	
	leucomycin	0.5-1	0.5	0.5-1	
lincosamides	lincomycin	**32**	0.125	**16-32**	**8-16**
	clindamycin	**16-32**	0.0156	**16**	**4-8**
pleuromutilins	tiamulin	**128**	0.0625	**128**	**32-64**
	retapamulin	**>64**	0.0156	**>64**	
streptogramins	virginiamycin M1	**>64**	4	**>128**	
	virginiamycin S1	8	8	8	
tetracyclines	tetracycline	0.5	0.25	0.25	

Table S2. Minimum inhibitory concentrations (MICs) of ribosome-targeting antibiotics against *S. aureus* expressing VgaA$_{LC}$ *S. aureus* strain SH1000, harbouring empty vector pRMC2 or pRMC2 expressing wild-type *vgaA$_{LC}$* or its mutants.

	MIC, µg/mL				
Construct (mutation)	lincomycin	clindamycin	tiamulin	retapamulin	virginiamycin M1
pRMC2	0.5	0.06	0.5	0.06	2
pRMC2: *vgaA$_{LC}$*	**16**	**2**	**8**	**4**	4
pRMC2: *vgaA$_{LC}$* (K_{208}A)	**16**	**2**	**16**	**8**	4
pRMC2:*vgaA$_{LC}$* (S_{211}A)	**16**	**2**	**16**	**4**	4
pRMC2:*vgaA$_{LC}$* (S_{212}A)	**8**	**2**	**16**	**8**	4
pRMC2:*vgaA$_{LC}$* (S_{213}A)	**2**	0.125	1	0.125	1
pRMC2:*vgaA$_{LC}$* (K_{216}A)	**8**	**0.5**	**4**	**1**	4
pRMC:*vgaA$_{LC}$* (K_{218}A)	**16**	**1**	**16**	**4**	4
pRMC2:*vgaA$_{LC}$* (V_{219}A)	**16**	**1**	**16**	**8**	2
pRMC2:*vgaA$_{LC}$* (W_{223}A)	**2**	0.125	1	0.125	1
pRMC2:*vgaA$_{LC}$* (F_{224}A)	0.5	0.06	0.25	0.06	1
pRMC2:*vgaA$_{LC}$* (S_{226}A)	**16**	**2**	**16**	**8**	4
pRMC2:*vgaA$_{LC}$* (K_{227}A)	**4**	**0.25**	1	0.125	2
pRMC2:*vgaA$_{LC}$* (G_{228}A)	**8**	**2**	**8**	**2**	2
pRMC2:*vgaA$_{LC}$* (K_{229}A)	**16**	**2**	**8**	**4**	4
pRMC2:*vgaA$_{LC}$* (K_{230}A)	**16**	**2**	**8**	**4**	4
pRMC2:*vgaA$_{LC}$* (R_{232}A)	**16**	**2**	**8**	**2**	4

Table S3. Minimum inhibitory concentrations (MICs) of ribosome-targeting antibiotics against *L. monocytogenes* EDG-*e* expressing VgaL (Lmo0919). 5 x 10^5 CFU/mL (approximately OD_{600} 0.0003) of *L. monocytogenes EDGe*, Δ*lmo0919* (markerless) strain with integrated empty pIMK3 plasmid, or with pIMK3 encoding VgaL or VgaL-HTF was used to inoculate BHI media supplemented with 50 µg/mL kanamycin to maintain the integrative pIMK3 plasmid, 1 mM IPTG to induce expression of VgaL as well as increasing concentrations of antibiotics. After 16-20 hours at 37 °C without shaking, the presence or absence of bacterial growth was scored by eye. The MIC values that exceed the empty vector control lacking chromosomal *lmo0919* are shown in bold.

		MIC, µg/mL			
antibiotic class	antibiotic	*L. monocytogenes* EDGe::pIMK3	*L. monocytogenes* EDGe::Δ*lmo0919* pIMK3	*L. monocytogenes* EDGe::Δ*lmo0919* pIMK3 *vgaL*	*L. monocytogenes* EDGe::Δ*lmo0919* pIMK3 *vgaL*^{HTF}
phenicols	chloramphenicol	4	4	4	4
oxazolidinones	linezolid	1	1	1	
macrolides	erythromycin	< 0.125	< 0.125	< 0.125	< 0.125
lincosamides	lincomycin	**2**	0.5	**4**	**4**
pleuromutilins	tiamulin	**16-32**	0.125	**32**	**16-32**
streptogramins	virginiamycin M1	**32**	4-8	**64**	**32**
	virginiamycin S1	1	1	1	1
tetracyclines	tetracycline	0.25	0.25	0.25	0.25

Table S4. Cryo-EM data collection, modelling and refinement statistics.

	E. faecalis **70S–LsaA**	***S. aureus*** **70S–P-tRNA**	***S. aureus*** **70S–VgaA$_{LC}$**	***L. monocytogenes*** **70S–VgaL**
Data collection				
Magnification (×)	130 000	165 000	165 000	165 000
Electron dose (e$^-$/Å^2)	38.0	26.3	26.3	28.28
Defocus range (μm)	−0.7–2.2	−0.7–1.9	−0.7–1.9	−0.8–2.0
Pixel size (Å)	1.041	0.82	0.82	0.82
Initial particles	61 009	165 827	165 827	83 340
Final particles	59 262	61 910	35 129	45 548
Average resolution (Å)	2.9	3.1	3.1	2.9
Model composition				
Atoms	144 982	139 909	145 651	144 492
Protein residues	5 753	5 330	5 783	5 715
RNA bases	4 627	4554*	4 647	4617
Refinement				
Map CC around atoms	0.85	0.89	0.88	0.86
Map CC whole unit cell	0.85	0.88	0.87	0.85
Map sharpening B	−35.42	−56.43	−62.31	−68.16
R.M.S. deviations				
Bond lengths (Å)	0.008	0.010	0.009	0.014
Bond angles (°)	0.906	0.947	0.933	1.082
Validation				
MolProbity score	1.74	1.73	1.76	1.75
Clash score	4.19	3.87	4.24	4.41
Poor rotamers (%)	0.02	0.07	0.06	0.04
Ramachandran				
Favoured (%)	90.48	89.88	89.64	90.76
Outlier (%)	0.16	0.02	0.05	0.02

*23S rRNA helices H76–H78 of the L1 stalk were flexible and not modelled.

Table S5. Strains and Plasmids used in this study. Plasmid and strain construction is described in detail in supplemental text. *Denotes a plasmid constructed by the PEP facility at Umeå University.

Strain	Description	Source
***L. monocytogenes* EDGe**	Wild-type serotype 1/2a strain	(Glaser *et al*, 2001)
***L. monocytogenes* EGDe::pIMK3**	EGDe with empty pIMK3 plasmid containing P_{help} promoter integrated at $tRNA^{Arg}$ locus	This work
***L. monocytogenes* EDGe::pIMK3*lmo0919*^{HTF}**	EGDe with VgaL-HTF overexpressed from the P_{help} promoter integrated at $tRNA^{Arg}$ locus	This work
***L. monocytogenes* EDGe::pIMK3*lmo0919*$^{EQ2\text{-}HTF}$**	EGDe with VgaL EQ2-HTF overexpressed from the P_{help} promoter integrated at $tRNA^{Arg}$ locus	This work
L. monocytogenes* EDGe::Δ*lmo0919	EGDe harboring a *lmo0919* marker less deletion lacking VgaL	This work
***L. monocytogenes* EDGe::Δ*lmo0919*::pIMK3**	EGDe::Δ*lmo0919* with empty pIMK3 plasmid containing P_{help} promoter integrated at $tRNA^{Arg}$ locus	This work
L. monocytogenes* EDGe::Δ*lmo0919*::pIMK3*lmo0919	EGDe::Δ*lmo0919* with VgaL overexpressed from the P_{help} promoter integrated at $tRNA^{Arg}$ locus	This work
***L. monocytogenes* EDGe::Δ*lmo0919*::pIMK3*lmo0919*^{HTF}**	EGDe::Δ*lmo0919* with VgaL-HTF overexpressed from the P_{help} promoter integrated at $tRNA^{Arg}$ locus	This work
***L. monocytogenes* EDGe:: Δ*lmo0919*::pIMK3*lmo0919*$^{HTF\text{-}EQ2}$**	EGDe::Δ*lmo0919* with VgaL-EQ2-HTF overexpressed from the P_{help} promoter integrated at $tRNA^{Arg}$ locus	This work
***E. faecalis* OG1RF**	Rif^r Fus^r; WT *E. faecalis*	(Singh *et al.*, 2002)
***E. faecalis* TX5332**	Rif^r Fus^r Kan^r; *lsa* gene disruption mutant (OG1RF *lsa*::pTEX4577)	(Davis *et al*, 2001)
***S. aureus* SH1000**	Functional *rsbU*$^+$ derivative of *S. aureus* 8325-4	(Horsburgh *et al.*, 2002; O'Neill, 2010)
***E. coli* S17.1**	*E. coli* strain used for conjugative plasmid transfer to *L. monocytogenes*	(Simon *et al*, 1983)

Plasmid	Description	Reference
pIMK3	Kan^r; Listerial tRNA^{Arg} locus specific integrative vector for high-level IPTG-induced protein expression from the P_{help} promoter	(Monk *et al*, 2008)
pMAD	Amp^r, Ery^r; *lacZ*; thermosensitive shuttle vector used for allelic exchange in *L. monocytogenes*	(Arnaud *et al.*, 2004)
pHT009	Amp^r, Km^r; thrC locus specific integrative vector for high-level IPTG-induced protein expression from the $P_{hy\text{-}spnak}$ promoter	(Crowe-McAuliffe *et al.*, 2018)
VHp689	pMAD Δ*lmo0919*	This work
VHp690	pIMK3:*lmo0919*	This work
VHp692	pIMK3:*lmo0919-HTF*	This work
VHp693	pIMK3:*lmo0919-EQ2-HTF*	This work
pTX5333	Cm^r; *E. faecalis-E. coli* shuttle plasmid expressing LsaA from native promoter	(Singh *et al.*, 2002)
pCIE	Cm^r; *E. faecalis-E. coli* shuttle plasmid for cCF10 induced expression of proteins	(Weaver *et al.*, 2017)
VHp100	pCIE:*lsaA-HTF*	This work*
VHp149	pCIE:*lsaA-EQ2-HTF*	This work*
VHp369	pHT009-*lsaA*	This work
VHp426	pCIE, Sc^r; Cm^r gene swapped to spectinomycin resistance (Sc^r) gene	This work*
VHp431	VHp426:*lsa*	This work*
VHp526	pHT009-*lsaA*K244A	This work
VHp526	pHT009-*lsaA*K244A	This work
pRMC2	Amp^r, Cm^r; *E. coli - S. aureus* shuttle plasmid for tetracycline-regulable expression of proteins in the latter host.	(Corrigan & Foster, 2009)
pRMC2:*vgaA-FLAG$_3$*	pRMC2 expressing C-terminally FLAG$_3$ tagged VgaA$_{LC}$	This work
pRMC2:*vgaA-EQ2-FLAG$_3$*	pRMC2 expressing C-terminally FLAG$_3$ tagged VgaA$_{LC}$-E$_{105}$Q, E$_{410}$Q	This work
pRMC2:*vgaA$_{LC}$*	pRMC2 expressing wild-type VgaA$_{LC}$	This work
pRMC2:*vgaA$_{LC}$* (K$_{208}$A)	pRMC2 expressing VgaA$_{LC}$ ^{K208A}	This work
pRMC2:*vgaA$_{LC}$* (S$_{211}$A)	pRMC2 expressing VgaA$_{LC}$ ^{S211A}	This work
pRMC2:*vgaA$_{LC}$* (S$_{212}$A)	pRMC2 expressing VgaA$_{LC}$ ^{S212A}	This work
pRMC2:*vgaA$_{LC}$* (S$_{213}$A)	pRMC2 expressing VgaA$_{LC}$ ^{S213A}	This work
pRMC2:*vgaA$_{LC}$* (K$_{216}$A)	pRMC2 expressing VgaA$_{LC}$ ^{K216A}	This work
pRMC2:*vgaA$_{LC}$* (K$_{218}$A)	pRMC2 expressing VgaA$_{LC}$ ^{K218A}	This work
pRMC2:*vgaA$_{LC}$* (V$_{219}$A)	pRMC2 expressing VgaA$_{LC}$ ^{V219A}	This work
pRMC2:*vgaA$_{LC}$* (W$_{223}$A)	pRMC2 expressing VgaA$_{LC}$ ^{W223A}	This work
pRMC2:*vgaA$_{LC}$* (F$_{224}$A)	pRMC2 expressing VgaA$_{LC}$ ^{F224A}	This work
pRMC2:*vgaA$_{LC}$* (S$_{226}$A)	pRMC2 expressing VgaA$_{LC}$ ^{S226A}	This work
pRMC2:*vgaA$_{LC}$* (K$_{227}$A)	pRMC2 expressing VgaA$_{LC}$ ^{K227A}	This work
pRMC2:*vgaA$_{LC}$* (G$_{228}$A)	pRMC2 expressing VgaA$_{LC}$ ^{G228A}	This work

pRMC2:*vgaA*$_{LC}$ (K$_{229}$A)	pRMC2 expressing VgaA$_{LC}$ ^{K229A}	This work
pRMC2:*vgaA*$_{LC}$ (K$_{230}$A)	pRMC2 expressing VgaA$_{LC}$ ^{K230A}	This work
pRMC2:*vgaA*$_{LC}$ (A$_{232}$A)	pRMC2 expressing VgaA$_{LC}$ ^{A232A}	This work

1598